



**GTI ENERGY**

*solutions that transform*

**REPORT**

GTI ENERGY PROJECT NUMBER 21513

---

**Pilot Test of a Nanoporous, Super-hydrophobic Membrane Contactor Process for Post-combustion CO<sub>2</sub> Capture**

**Work Performed Under Agreement:**

DOE Contract No. DE-FE0012829

**Authors:**

Shiguang Li, Howard Meyer, Travis Pyrzynski, GTI Energy  
Ed Sanders, Uttam Shanbhag, Air Liquide Advanced Separations

**Report Issued:**

October 6, 2022

**Prepared For:**

National Carbon Capture Center (Host Site), and  
U.S. Department of Energy, National Energy Technology Laboratory

**DOE Project Manager:**

Mr. Andrew O’Palko, Project Manager  
National Energy Technology Laboratory  
3610 Collins Ferry Rd. Morgantown, WV 26505  
(304) 285-4715  
andrew.opalko@netl.doe.gov

**GTI Energy Technical Contact:**

Dr. Shiguang Li  
R&D Program Manager, Separations, GTI Energy  
(847) 544-3478  
SLi@gti.energy

1700 S. Mount Prospect Rd.  
Des Plaines, Illinois 60018  
www.gti.energy

## Legal Notice

---

*This information was prepared by GTI Energy for the National Carbon Capture Center.*

*Neither GTI Energy, the members of GTI Energy, the Sponsor(s), nor any person acting on behalf of any of them:*

*a. Makes any warranty or representation, express or implied with respect to the accuracy, completeness, or usefulness of the information contained in this report, or that the use of any information, apparatus, method, or process disclosed in this report may not infringe privately-owned rights. Inasmuch as this project is experimental in nature, the technical information, results, or conclusions cannot be predicted. Conclusions and analysis of results by GTI Energy represent GTI Energy's opinion based on inferences from measurements and empirical relationships, which inferences and assumptions are not infallible, and with respect to which competent specialists may differ.*

*b. Assumes any liability with respect to the use of, or for any and all damages resulting from the use of, any information, apparatus, method, or process disclosed in this report; any other use of, or reliance on, this report by any third party is at the third party's sole risk.*

*c. The results within this report relate only to the items tested.*

## **Table of Contents**

---

Legal Notice .....	2
Table of Contents.....	2
1. Executive Summary .....	4
2. Introduction .....	6
3. Materials and Experimental Method .....	8
4. System Installation at NCCC .....	13
5. Results and Discussions .....	15
6. Decommissioning of HFMC System.....	48
7. Summary of Lessons Learned and Improvements .....	49
8. Summary of Accomplishments and Contribution .....	51
9. Conclusions and Future Steps .....	52
10. References.....	53
List of Acronyms .....	54

## 1. Executive Summary

---

GTI Energy and Air Liquide Advanced Separations (ALaS) have been developing a novel hollow fiber membrane contactor (HFMC) technology for post-combustion CO<sub>2</sub> capture. The process combines advantageous features of both absorption and membrane processes to cost-effectively separate CO<sub>2</sub> from flue gas. In the absorption step, flue gas is sent through the hollow fiber membrane tubes while a CO<sub>2</sub>-selective solvent flows around the outer surface of the hollow fiber membrane tubes, allowing CO<sub>2</sub> to permeate through the membrane and be absorbed into the solvent. In the desorption step of the process, the CO<sub>2</sub>-rich solvent is regenerated and sent back to the membrane absorber.

The key component of the HFMC process is the super-hydrophobic, porous hollow fiber, which is made from poly(ether ether ketone) (PEEK). PEEK is an engineering polymer with thermo-mechanical properties and chemical resistance superior to most commercial plastics, including typical polymers used in membrane fabrication. The unique characteristics of PEEK allow the HFMC device to be utilized successfully in challenging and aggressive chemical environments. These properties, combined with super-hydrophobicity, enable PEEK HFMC to overcome pore wetting and chemical durability problems that have plagued prior HFMC technologies.

Compared to conventional absorption/desorption technologies, the critical advantage of the HFMC process is the high contact surface area provided by the hollow fibers that enables an increased volumetric mass-transfer rate. In the PEEK HFMC process, the specific surface area has been increased by an order of magnitude over structurally packed or trayed columns, resulting in compact systems with small footprints.

Supported by the U.S. Department of Energy (DE-FE0012829), a pilot-scale demonstration of the HFMC process on a coal-fired power plant flue gas has been performed in Wilsonville, AL at the National Carbon Capture Center (NCCC). In this project, the PEEK HFMC technology was scaled from the bench scale to a pilot scale (0.5 MW<sub>e</sub> equivalent CO<sub>2</sub> capture system) utilizing 28 commercial-sized membrane modules. Each module is measured 8-inches-diameter by 5-feet-long with a membrane surface area of about 35 m<sup>2</sup> per module. These modules have shown high CO<sub>2</sub> capture rates due to the high membrane intrinsic CO<sub>2</sub> permeance as well as the structured PEEK hollow fiber module configuration. In this study, CO<sub>2</sub> gas permeance of 2,150 GPU [1 GPU = 10<sup>-6</sup> cm<sup>3</sup>(STP)/(cm<sup>2</sup>·s·cmHg)] was attained by optimizing the membrane preparation procedures. By using a 50 wt.% aqueous activated methyl diethanolamine (aMDEA) solvent, the HFMC showed >90 vol% CO<sub>2</sub> removal and >98 vol% CO<sub>2</sub> product purity during tests in the laboratory with simulated flue gas. A skid containing 28 membrane

modules and two-stage regeneration with a reboiler and flash vessel for each stage was designed, constructed, and installed at NCCC.

A 90% CO<sub>2</sub> removal rate was achieved by the HFMC using a 50 wt.% aMDEA solvent during the initial tests with 4 modules and actual coal-fired flue gas at NCCC. The stripped stream from the two-stage flash desorber has a CO<sub>2</sub> concentration of >98.6 vol%. Further tests indicated an issue of liquid-side concentration polarization – higher CO<sub>2</sub> concentration in the fluid boundary layer (next to the fiber) relative to the bulk flow stream. This issue was resolved by decreasing the aMDEA concentration from 50 wt.% to 35 wt.%.

Parametric tests were then conducted to investigate the effects of flue gas temperature, solvent temperature, flue gas feed pressure, and solvent flow velocity on CO<sub>2</sub> capture performance. Based on the parametric testing, the operating conditions for full-scale (28 modules) and 2-month continuous testing were determined.

Continuous testing with 28 membrane modules, however, did not match the single module results; the CO<sub>2</sub> capture performance declined with time. Quantitative analysis as well as inspection and measurements of the spent modules were conducted to investigate the potential causes. The major issue identified was the tubesheet leaking from patch points and potentially from fiber/epoxy separation due to non-uniform bonding. Corrective actions addressing cartridge shortcomings have been developed and incorporated into the fabrication of four membrane bundles. The resulting four membranes were tested at NCCC. The results indicated that the decline trends for CO<sub>2</sub> removal rate and CO<sub>2</sub> removal flux were identical to those of the previous tests conducted in 2018 and 2021. Analysis of the fiber and tubesheet identified no specific defects or any loss in hydrophobicity of the super-hydrophobic coating that could directly be attributed to the liquid leakage seen during the field operation. Tubesheet leaking, while smaller in size (volumetrically) than previously tested contactors, was clearly evident. The lack of improvement of the CO<sub>2</sub> capture performance and stability of this performance indicates that not all leak paths were addressed and/or additional mechanisms were responsible for it. Moving forward, technical hurdles in materials and manufacturing will need to be resolved in a bench-scale program.

## 2. Introduction

---

The pilot-scale test project is a continuation of GTI Energy's bench-scale technology development (October 1, 2010 – December 31, 2013) supported by DOE (DE-FE-0004787). The hollow fiber membrane contactor (HFMC) process combines advantageous features of both absorption and membrane processes to provide a cost-effective solution for CO<sub>2</sub> capture from flue gases. In this process, CO<sub>2</sub>-containing flue gas passes through one side of the PEEK HFMC, while a CO<sub>2</sub>-selective solvent flows on the other side. CO<sub>2</sub> permeates through the hollow fiber membrane pores and is chemically absorbed into the solvent. The CO<sub>2</sub>-rich solvent is then regenerated and sent back to the membrane absorber.

The membrane contactor process is different from a conventional membrane process, which operates by a solution/diffusion mechanism where the separation driving force is provided by the partial pressure difference of each component across the membrane. This process requires either flue gas compression, permeate sweep, application of a permeate-side vacuum, or a combination of these steps to provide a sufficient separation driving force. Elaborate process design and optimization become a prerequisite for a conventional membrane process in CO<sub>2</sub> capture from flue gases.<sup>1</sup> The main limitation of conventional membrane processes is the process pressure ratio (feed gas pressure/permeate gas pressure) limitation. Multiple membrane stages may be required to generate greater than 95% pure CO<sub>2</sub> product (DOE's target) from flue gases using the conventional membrane process.

In the hybrid membrane/absorption process, the permeate-side partial pressure of CO<sub>2</sub> can be considered to be close to zero due to the chemical reaction of CO<sub>2</sub> with the absorption solvent, and thus overcomes the pressure ratio problem encountered by the conventional gas membrane process. Neither feed compression or permeate vacuum are required to create the separation driving force for gas molecules to be transported through the membrane. The process selectivity for the hybrid membrane/absorption process is determined by the chemical affinity of the absorption solvent to CO<sub>2</sub>. Therefore, a high-purity CO<sub>2</sub> product can be realized in a single-stage hybrid membrane/absorption process.

The use of HFMCs for CO<sub>2</sub> capture, especially the absorption process, has been a subject of intense research interest because they provide a very high surface area to volume ratio for the separation to take place.<sup>2-6</sup> This leads to a mass transfer coefficient that is 5 to 10 times greater than that can be achieved in a conventional tower or column with trays or packing. Thus, the use of a membrane contactor instead of a conventional amine scrubber tower leads to a much smaller space requirement. This technology is well suited for new and existing Pulverized Coal (PC) power plants due to the reduced footprint requirement and a much lower visual impact, as well as providing

more options for placement in the confines of existing plants.

The Project Team is comprised of GTI Energy, ALaS, and Trimeric Corporation. This slipstream test project utilizes each Team Member's unique expertise (GTI Energy: HFMC process technology, ALaS: commercial-sized PEEK membrane and module fabrication, and Trimeric: Techno-Economic Analysis) that is critical to scaling up the HFMC technology.

The main objectives of the pilot-scale development of the PEEK HFMC system at the NCCC site in Wilsonville, AL were as follows:

- Build a 0.5 MW<sub>e</sub> equivalent pilot-scale CO<sub>2</sub> capture system using PEEK hollow fibers in a membrane contactor and conduct tests on flue gas at the NCCC;
- Demonstrate a continuous, steady-state operation for a minimum of two months; and
- Gather data necessary for further process scale-up.

The goal of the testing at NCCC is to achieve DOE's Carbon Capture performance goal of 90% CO<sub>2</sub> capture rate with 95% CO<sub>2</sub> purity at a cost of \$40/tonne of CO<sub>2</sub> captured by 2025.

The main scope of work at NCCC was as follows:

- Complete site preparation, system installation, and on-site system shakedown;
- Perform parametric tests and identify operational conditions for the continuous steady-state run;
- Complete a continuous, steady-state operation for a minimum of two months, gather data necessary for further process scale-up; and
- Remove the skid from the testing site.

### 3. Materials and Experimental Method

#### 3.1. PEEK fibers

Polyether ether ketone (PEEK, chemical formula shown in Figure 1) is a commercial “best in class” plastic with thermo-mechanical properties and chemical resistance superior to essentially all commercial plastics.<sup>7</sup> The unique characteristics of PEEK are due to the semi-crystalline nature of the polymer. Table 1 compares the thermo-mechanical properties of PEEK with other typical membrane materials.<sup>8</sup> The maximum service temperature is as high as 520°F (271°C).

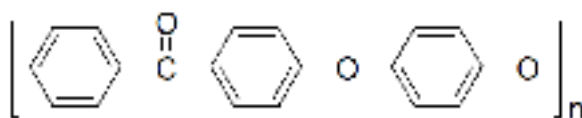


**Figure 1.** PEEK structural formula.

**Table 1.** Thermo-mechanical properties of membrane forming polymer.

Polymer	Tensile modulus (GPa)	Tensile strength (MPa/kpsi)	Max service temperature (°C/°F)
Teflon™	0.4-0.5	17-21/2.5-3.0	250/480
PVDF	0.8	48/7.0	150/302
Polysulfone	2.6	70/10.2	160/320
PEEK	4	97/14.1	271/520

Commercial-scale production equipment (Figure 2: fiber extrusion lines, and Figure 3: composite hollow fiber production lines) is used in the production of PEEK fibers.



**Figure 2.** PEEK hollow fiber extrusion lines.



**Figure 3.** Fiber production lines.



### 3.2. Membrane module construction

The placement of the hollow fiber within the module was controlled through computer-controlled helical fiber winding. The process generates a structured packing configuration minimizing channeling, bypassing, and minimizing concentration polarization. A wound cartridge with a controlled uniform structured packing is shown in Figure 6. The hollow fibers are arranged in a helical path, with the axis of the fibers running confluent to the principal direction of fluid flow. To enable the use of a counter-current flow configuration, which is thermodynamically most efficient, the packing density in the cartridge must be uniform. Also, flow bypassing, and entrance and exit effects must be minimized. The fiber packing density and packing uniformity were controlled to ensure an optimal flow distribution with minimal pressure drop on both the feed and the permeate sides. Figure 7 shows an 8-inch-diameter membrane cartridge used in the current study. Each cartridge measured 5-feet-long with a membrane surface area of about 30-40 m<sup>2</sup> per module.



**Figure 6.** Helically wound structured hollow fiber cartridge.



**Figure 7.** Photograph of 8-inch diameter membrane cartridges.

The membrane cartridge was sealed with O-rings and housed in a stainless-steel pressure vessel. Membrane intrinsic CO<sub>2</sub> permeance is important in attaining high CO<sub>2</sub> capture rates in membrane contactor mode. By modifying and optimizing membrane preparation procedures and module construction conditions, membrane intrinsic CO<sub>2</sub> permeances as high as 2,000-2,670 GPU (1 GPU = 10<sup>-6</sup> cm<sup>3</sup> (STP)/(cm<sup>2</sup>·s·cmHg)) were achieved as shown in Table 2. Table 2 also lists the effective area and specific area of the bundles for each of the modules fabricated.

**Table 2.** Intrinsic permeances for CO<sub>2</sub> through 8-inch-diameter modules.

Module	Cartridge diameter (inch/cm)	Membrane effective inside area (m <sup>2</sup> )	Bundle porosity (%)	Specific area of bundle (m <sup>2</sup> /m <sup>3</sup> )	Module intrinsic CO <sub>2</sub> permeance (GPU*)
8PG-58-142	8/20	37.6	59.4	1,560	2,670
8PG-3034	8/20	31.8	63.5	2,620	2,150

\*: 1 GPU = 10<sup>-6</sup> cm<sup>3</sup> (STP)/(cm<sup>2</sup>·s·cmHg).

### 3.3. Membrane contactor CO<sub>2</sub> capture testing

A process flow diagram is shown in Figure 8, which shows how the CO<sub>2</sub> capture process pilot was integrated with the flue gas at the NCCC's pilot Bay 2. The flue gas is sent to a blower, which boosts the flue gas pressure to approximately 1-20 psig. The flue gas is then filtered and sent to the HFMC absorber. CO<sub>2</sub> permeates through the membrane and is absorbed in the solvent. The CO<sub>2</sub>-rich solvent is regenerated by a two-stage regeneration using a reboiler and flash vessel for each stage. Both treated flue gas and stripped CO<sub>2</sub> streams from the desorber were returned upstream of Plant Gaston's Flue Gas Desulfurization (FGD) unit.

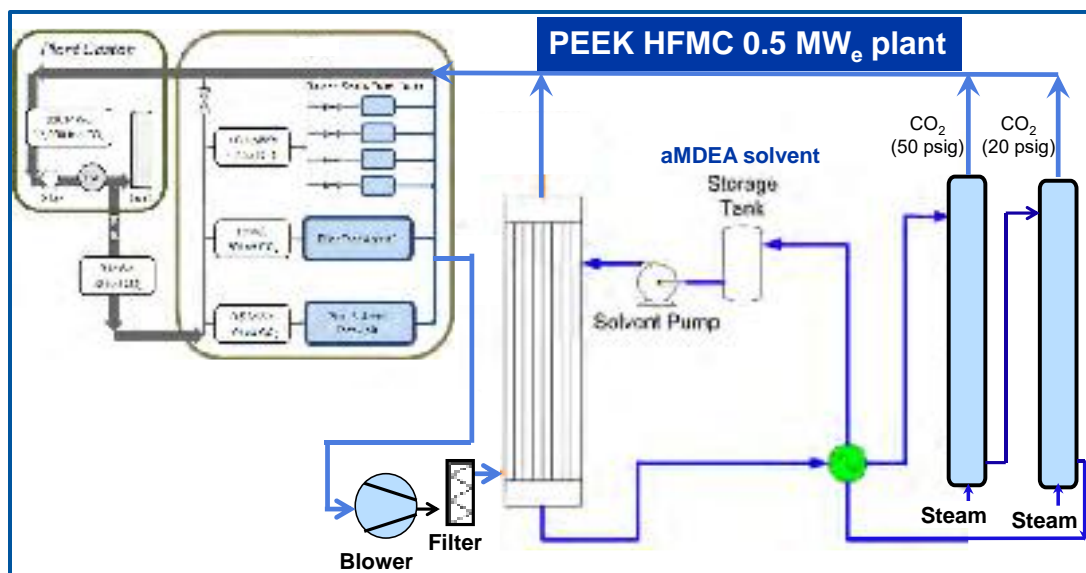


**Figure 8.** Process flow diagram.

During the membrane contactor CO<sub>2</sub> capture tests, the following measurements were conducted to collect the data:

### **3.3.1. Compositions of the feed and treated flue gases**

The compositions of the feed and treated flue gases compositions were measured by a Horiba PG-350 flue gas analyzer. NCCC personnel ordered calibration gases, including calibration standards for CO<sub>2</sub>, CO, NO, SO<sub>2</sub>, O<sub>2</sub>, and zero gas (N<sub>2</sub>). NCCC personnel also provided GTI Energy with additional calibration standards that they had available when different mixtures were requested to test different calibration points.

### **3.3.2. CO<sub>2</sub> loading analysis**

NCCC analytical staff analyzed 50 activated MDEA samples for CO<sub>2</sub> loading. The analysis was initially done using a total inorganic carbon (TIC) analysis method. The instrument was down for some time, and during that time, samples were analyzed using a titration method. Once the TIC instrument was up and running, the analysis was repeated by TIC. The lean amine samples had a typical CO<sub>2</sub> loading in the range of 0.5-1 wt.% CO<sub>2</sub>, and the average loading was 0.77 wt.%. The rich samples had a CO<sub>2</sub> loading in the range of 2-5 wt.%.

### **3.3.3. Solvent concentration**

During the test campaign, the solvent concentration was measured by two different methods - Karl Fischer analysis (K-F) and GC analysis. For K-F, the water content was directly measured. For GC analysis, the active amine components were identified and then measured, allowing the water concentration to be determined by subtracting the amine concentration and CO<sub>2</sub> loading. The K-F was done exclusively during 2017, after which solvent analysis was conducted by GC. Periodically, K-F was conducted to verify the measurements. In addition to the bulk solvent, some samples were collected during the test run to verify if the liquid contained solvent. For example, liquid collected as condensate on the gas side of the membranes was analyzed to determine if that mixture contained any solvent that may have permeated to the gas side.

### **3.3.4. Composition of the solvent regeneration flash gas**

NCCC personnel set up a gas chromatograph (GC) for testing the composition of the flash gas from the regeneration process. This included setting up and calibrating the GC and setting up sample lines, including valves and a condenser to remove any liquid before the sample reaches the GC. GTI Energy personnel switched the valves and recorded concentrations when data was collected. The CO<sub>2</sub> concentration was typically in the range of 96%-99.9% CO<sub>2</sub>. Data were collected during each test run.

#### 4. System Installation at NCCC

Based on discussions with NCCC, the pilot plant was installed at NCCC's Pilot Bay 2 West (Figure 9).

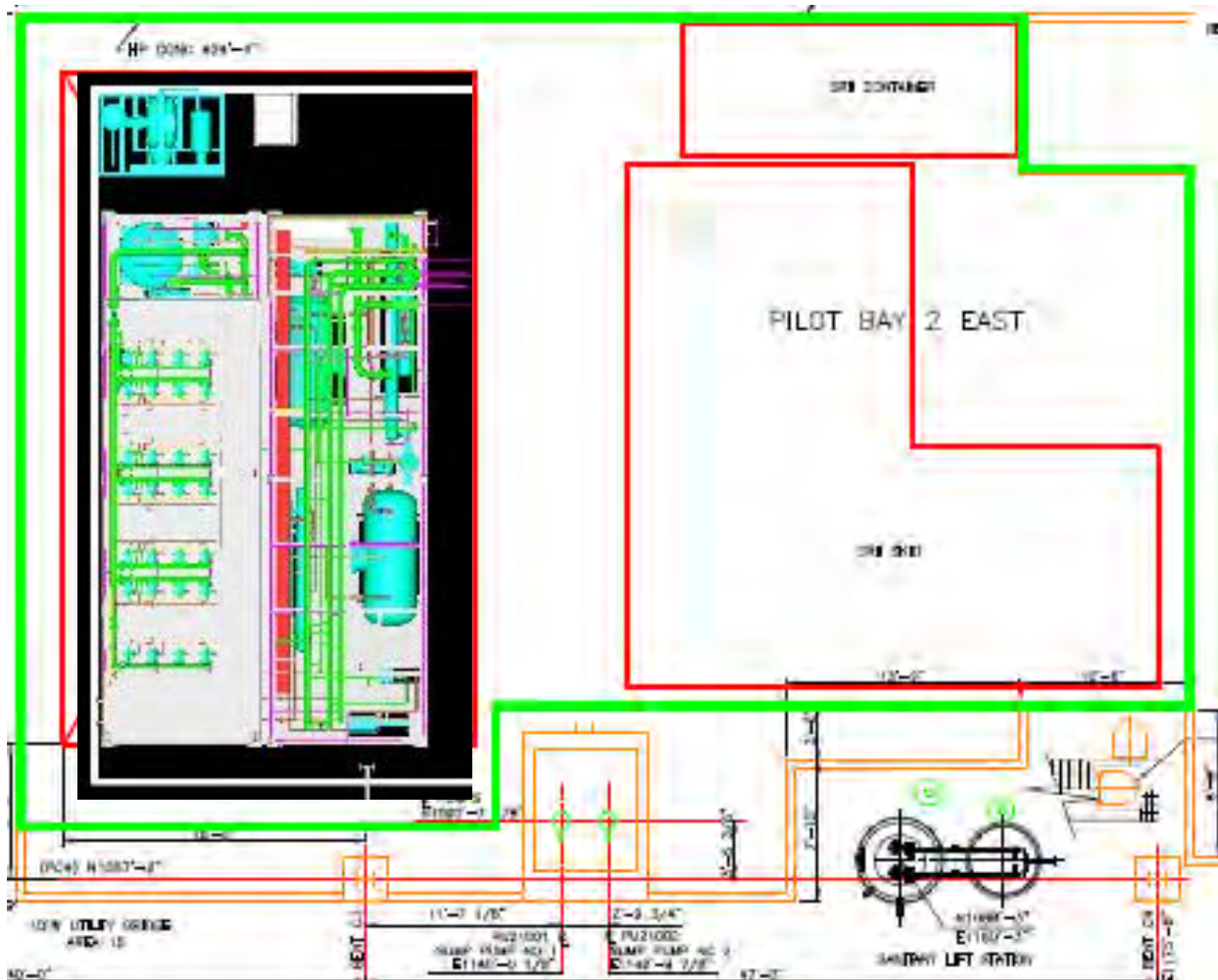


**Figure 9.** Layout of the 0.5 MWe PEEK HFMC plant.

The skids constructed by EPIC System, Inc. in St. Louis, MO were shipped on three trucks, two oversize load- and one standard. The trucks arrived at NCCC on March 15, 2017 (Figure 10).

The skids were unloaded from each of the flatbed trucks and then set in place using a crane (Figure 11). The team that helped with the installation of the skids included ironworkers and pipefitters, and NCCC engineers. The team was able to set all four skids safely and without any major issues. Figure 12 shows the installed HFMC system.



**Figure 10.** Skids arrived at NCCC.



**Figure 11.** Setting of skids.

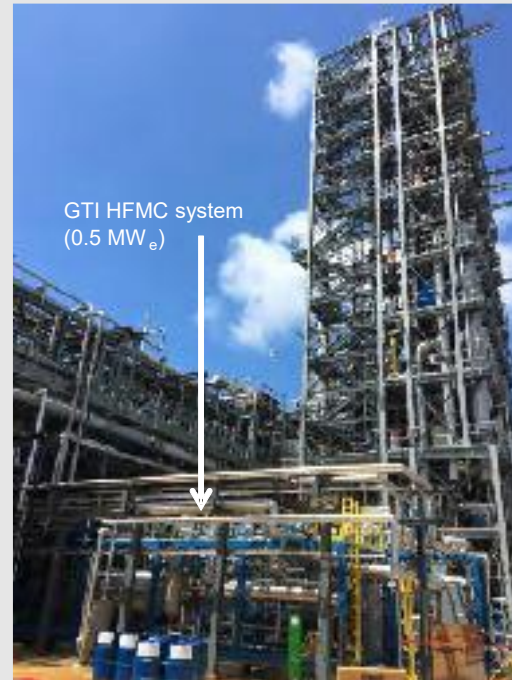


**Figure 12.** Installed HFMC system.

## 5. Results and Discussions

### 5.1. Commissioning tests

After the completion of the commissioning, flue gas CO<sub>2</sub> capture performance testing was conducted for the four membrane modules installed in the system using a 50 wt.% aMDEA solvent. Early testing results with real flue gas at NCCC indicated a 90% CO<sub>2</sub> capture rate can be achieved by adjusting the flue gas inlet flow rate (Figure 13). The stripped stream from the two-stage flash desorber had a CO<sub>2</sub> concentration of >98.6 vol%.

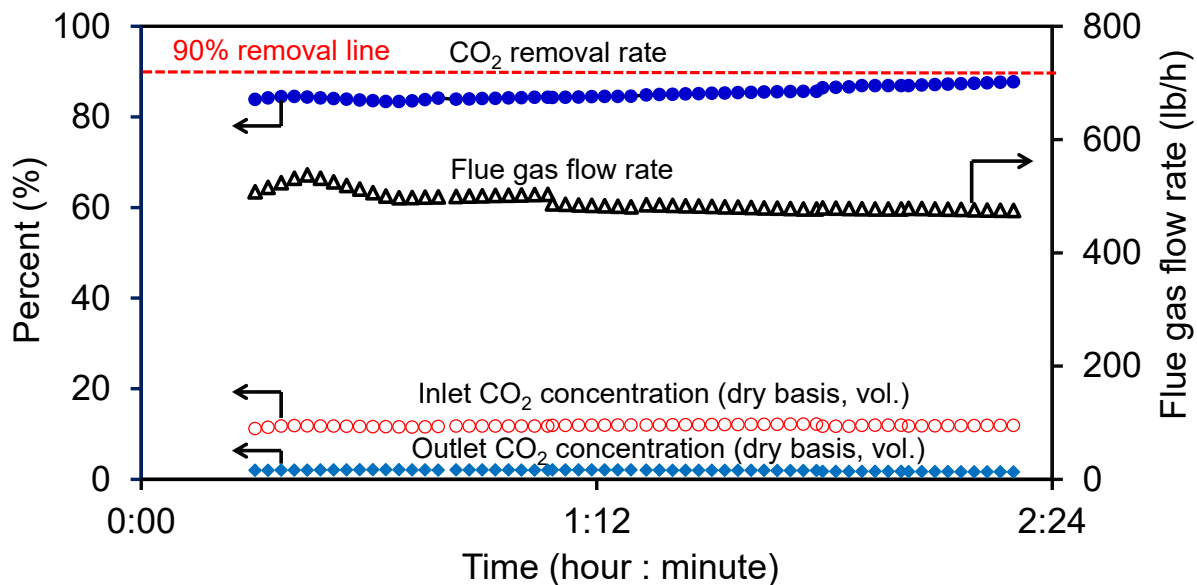


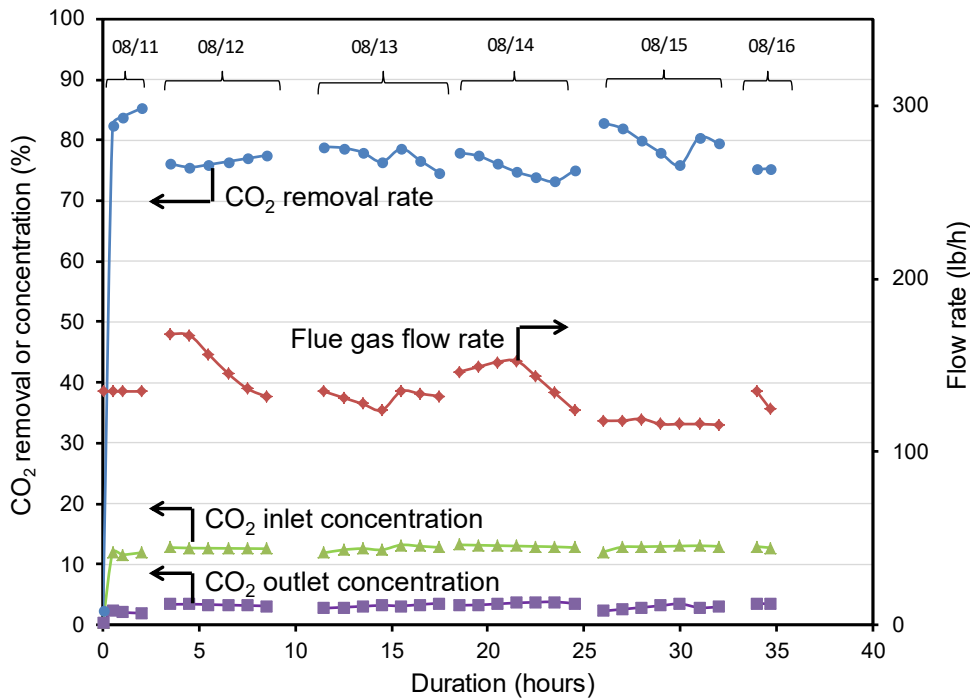
**Figure 13.** Run chronology for one (of seven) membrane "clusters" in service after 6 hours of operation.

Startup/shutdown performance was then investigated using a single module instead of four modules. The startup/shutdown procedure was as follows:

- **Startup:** 1) turn on the blower, 2) wait until the flue gas flow rate is stabilized, and 3) turn on the liquid pump
- **Shutdown:** 1) shut off the liquid pump, 2) shut off the blower, and 3) drain out the shell-side liquid

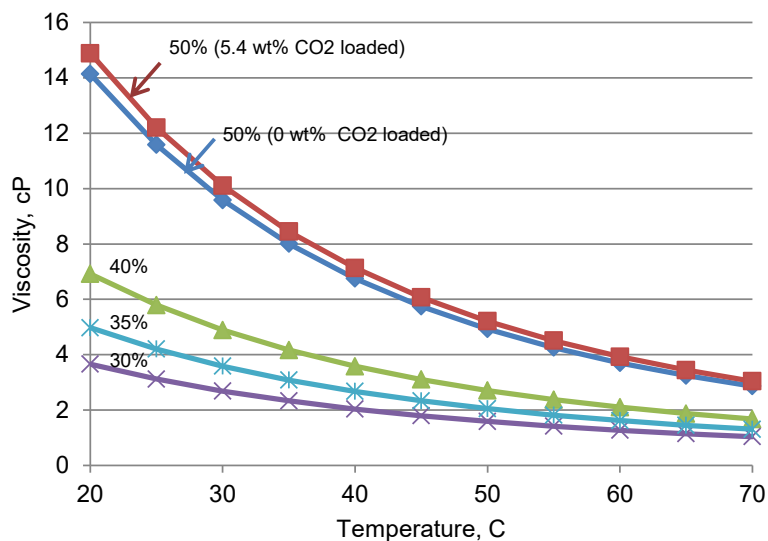
During the tests, the CO<sub>2</sub> absorption continued to run for 1-2 hours and steady-state CO<sub>2</sub> permeation flux was monitored. During the shutdown procedure, after CO<sub>2</sub> removal performance tests, the liquid side and gas side pressures were released, a small amount of N<sub>2</sub> was blown on the gas side, and the liquid side solvent was drained. This was carried out for a couple of days after which the module was tested again for CO<sub>2</sub> removal performance. Figure 14 shows that the first data point collected every day was always higher than the last data point collected on the previous day. This is typical of

liquid-side concentration polarization – higher CO<sub>2</sub> concentration in the fluid boundary layer (next to the fiber) relative to the bulk flow stream.



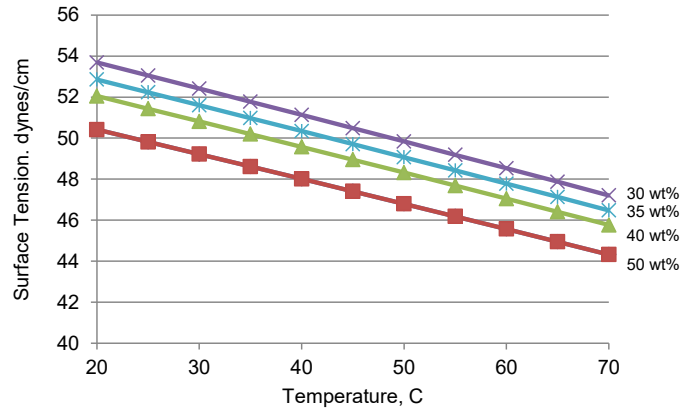
**Figure 14.** CO<sub>2</sub> removal rate, flue gas flow rate, and CO<sub>2</sub> inlet and outlet concentrations as functions of duration for a single 8-inch-diameter module.

To resolve the issue of liquid-side concentration polarization, an approach proposed was to decrease solvent amine concentration from 50 wt.% to 35 wt.%. As shown in Figure 15, the solvent viscosity significantly decreased as the amine concentration decreased from 50 wt.% to 30 wt.%.



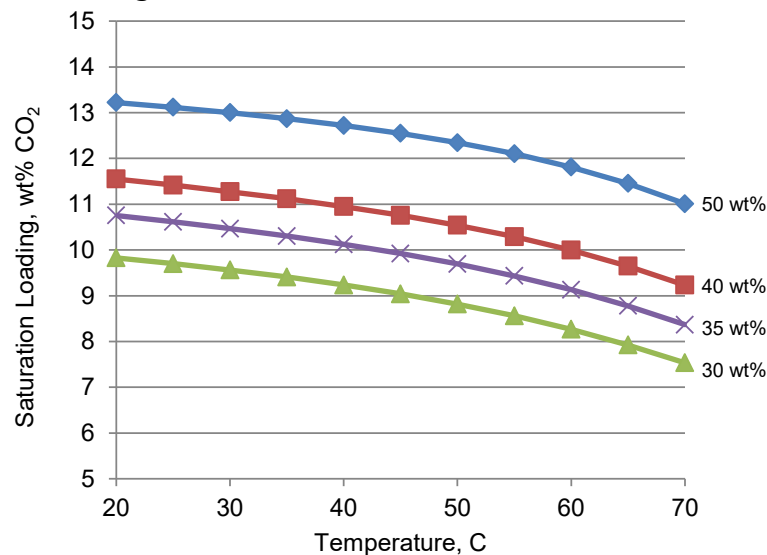
**Figure 15.** Solvent viscosity as a function of temperature.

Figure 16 shows solvent surface tension increased with decreasing amine concentration. Please note that higher surface tension provides higher breakthrough pressure in the HFMC. Therefore, the change of amine concentration from 50 wt.% to 35 wt.% for the solvent moves in the correct direction for reducing both liquid-side concentration polarization and membrane wetting.



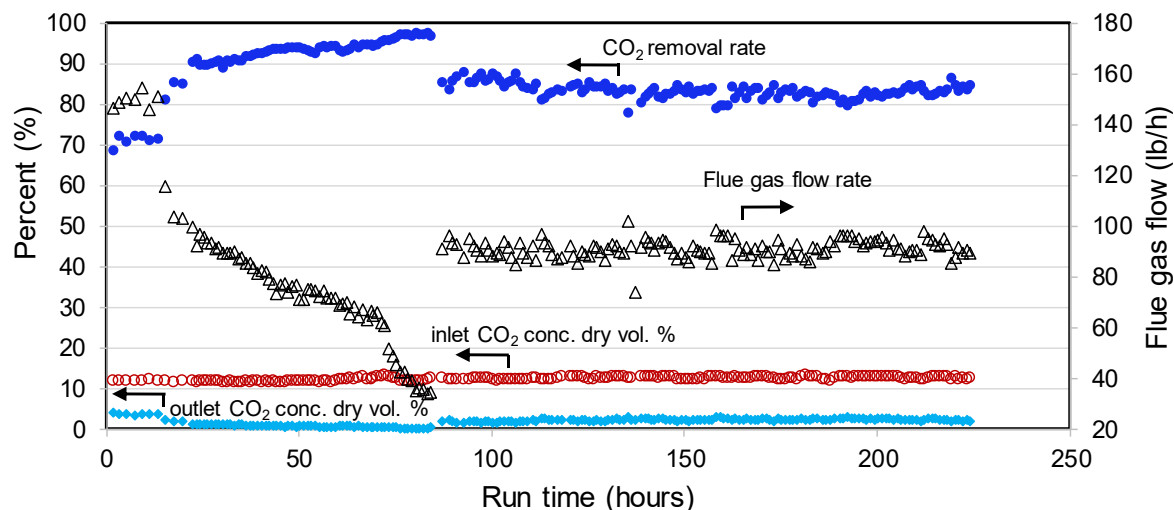
**Figure 16.** Solvent surface tension as a function of temperature.

Figure 17 shows solvent saturation loading decreases with decreasing amine concentration. For treating the same amount of CO<sub>2</sub> using the PEEK HFMC process, although the CO<sub>2</sub> loading in weight percent of the rich solvent remains unchanged as amine concentration decreases, the CO<sub>2</sub> loading in terms of mole CO<sub>2</sub> absorbed/mole amine of the rich solvent increases. The tradeoffs between viscosity, surface tension, and amine strength were evaluated, and down-selected 35 wt.% aMDEA for the future membrane contactor testing.



**Figure 17.** Solvent saturation loading as a function of temperature.

The 35 wt.% aMDEA solvent was then tested at NCCC with an 8-inch-diameter module (PG170055) installed into the pilot unit cluster A. The unit startup began on December 9, 2017. The GTI Energy team shut down the system on December 20, 2017. By then, 224-h of continuous testing was completed (Figure 18).



**Figure 18.** Run chronology for a single 8-inch-diameter module at NCCC.

The 224-h continuous testing had been successful. During the operation, the CO<sub>2</sub> inlet concentration was between 11.7-12.7 vol% (dry basis). The CO<sub>2</sub> capture rate increased with decreasing flue gas flow rate, as shown in Figure 18, for the first 83 hours. After 83 hours, the operation conditions, including the flue gas flow rate, were kept constant. A stable CO<sub>2</sub> capture performance was achieved. The steady-state CO<sub>2</sub> capture rate is about 83%. The 224-h testing also confirmed the liquid side concentration polarization issue observed previously had been resolved due to the change of solvent concentration from 50 wt.% to 35 wt.%.

## 5.2. Parametric tests

Parametric tests were then conducted to investigate the effects of flue gas temperature, solvent temperature, flue gas feed pressure, and solvent flow velocity on CO<sub>2</sub> capture performance. In such tests, a single module (8-inch-diameter) was used in conjunction with an aMDEA solvent (~35 wt.% amine). The typical operating conditions for the integrated absorption/desorption testing are listed in Table 3. As a note, to ensure a smooth operation on the regeneration section, the bulk solvent flow rate was 95 L/min while a slipstream of the solvent, 5.7 L/min, was sent to a single membrane. The typical operating procedure for parametric testing is as follows:

- 1) Adjust process condition to set point
- 2) Allow the system to run for at least 1 hour at the set point condition
- 3) Record system performance at that condition

**Table 3.** Operating conditions for the integrated absorption/desorption testing.

Parameter	Condition
<b>Membrane Absorption</b>	
Membrane contactor surface area	40 m <sup>2</sup>
Flue gas inlet temperature	119 - 144 °F
Flue gas composition	12% CO <sub>2</sub> , 8% O <sub>2</sub> , 80% N <sub>2</sub>
Flue gas inlet pressure	5 -13 psig
Solvent flow rate	5.7 L/min
Solvent inlet temperature	80 - 109 °F
Solvent inlet pressure	15 psig
<b>Desorption</b>	
Solvents	aMDEA/H <sub>2</sub> O (35 wt.%)
Liquid flow rate	95 L/min
1 <sup>st</sup> stage Solvent flash vessel temperature	247 °F
1 <sup>st</sup> stage Solvent flash vessel pressure	26 psig
2 <sup>nd</sup> stage solvent flash vessel temperature	270 °F
2 <sup>nd</sup> stage solvent flash vessel pressure	27 psig

### 5.2.1. Flue gas feed pressure

The flue gas feed gas pressure varied between 5.0 and 13.0 psig. The results are shown in Figure 19. The CO<sub>2</sub> capture flux increased with increasing feed pressure between 5.0 and 10.7 psig. As the CO<sub>2</sub> partial pressures gradient between the gas side and the liquid side increased, the CO<sub>2</sub> removal rate also increased, going from 80.5% at 5 psig to 89.0% at 10.7 psig. When the pressure was further increased from 10.7 to 13 psig, no noticeable difference was observed.

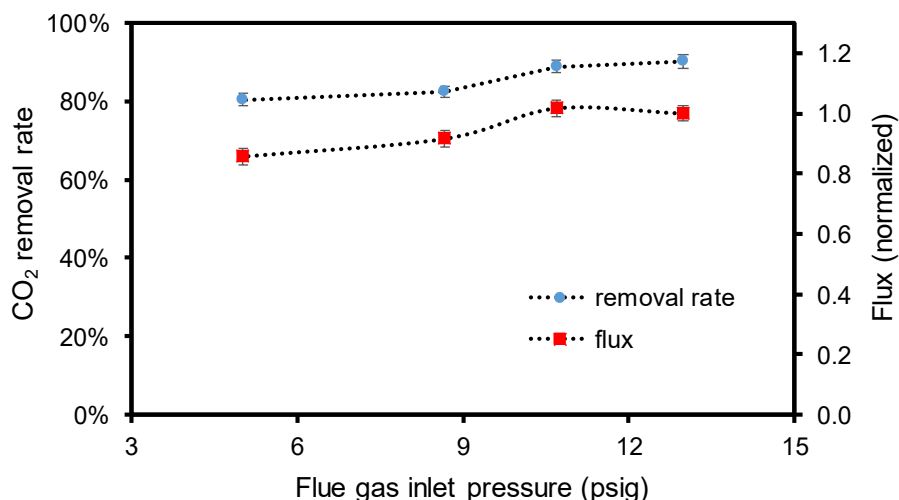


**Figure 19.** Normalized CO<sub>2</sub> flux and removal rate at 119 °F as a function of gas feed pressure. Gas side: 12.% CO<sub>2</sub> concentration; liquid side: 15 psig inlet pressure, 91 °F inlet temperature, and 5.8 L/min flow rate.

### 5.2.2. Flue gas feed temperature

The flue gas feed temperature varied between 119 and 144 °F. The results, shown in Figure 20, do not show a significant difference in CO<sub>2</sub> removal rate or flux in the temperature range tested.

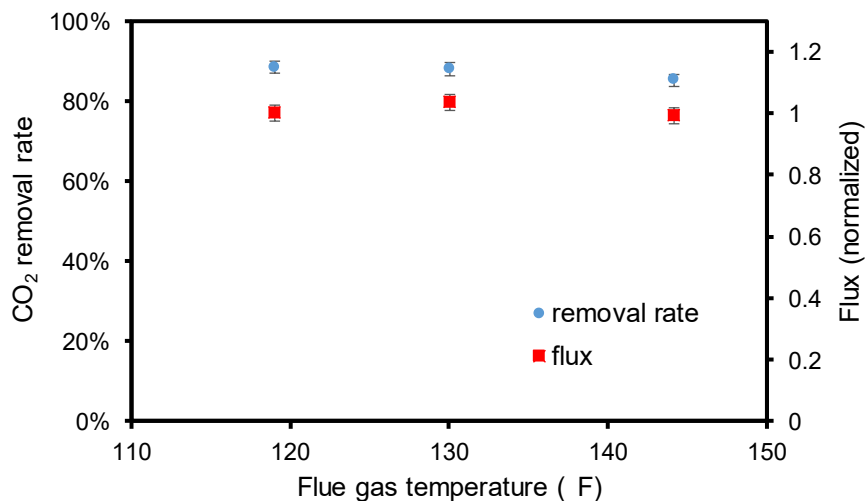


**Figure 20.** Normalized CO<sub>2</sub> flux and removal rate of flue gas as a function of flue gas temperature. Gas side: 12% CO<sub>2</sub> concentration and 13.0 psig feed pressure; liquid side: 11.8 psig inlet pressure, 91 °F inlet temperature, and 5.6 L/min flow rate.

### 5.2.3. Solvent linear flow velocity

Figure 21 shows that the normalized CO<sub>2</sub> flux increases with increasing solvent flow velocity. This is because the increase in solvent flow velocity increases turbulence for mass transport and thus decreases the liquid side resistance. Due to the increase in CO<sub>2</sub> flux, the CO<sub>2</sub> removal rate increased.

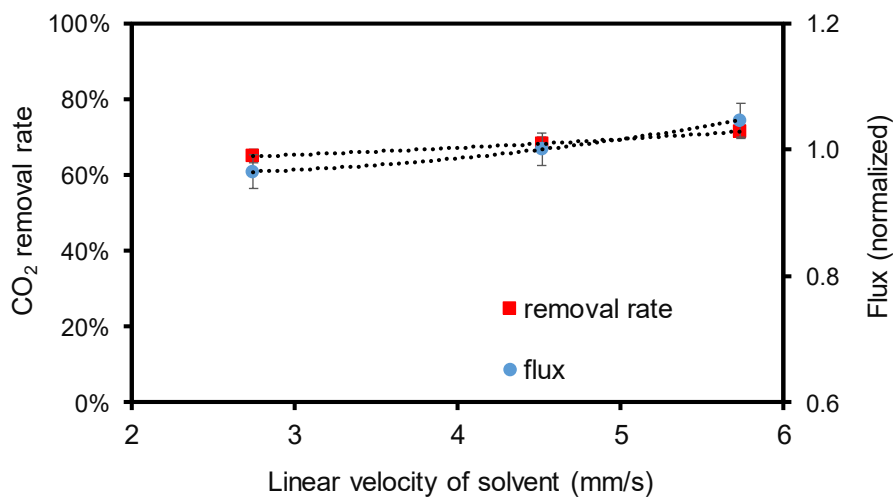


**Figure 21.** Normalized CO<sub>2</sub> flux and removal rate of flue gas at 136 °F as a function of solvent linear flow velocity. Gas side: 11.5% CO<sub>2</sub> concentration and 12 psig feed pressure; liquid side: 20 psig inlet pressure, 88 °F inlet temperature, and 5.9 L/min flow rate.

### 5.2.4. Solvent temperature

The solvent inlet temperature varied from 80 to 111 °F. The results are shown in Figure 22. In the temperature range tested, there was no significant difference in performance.

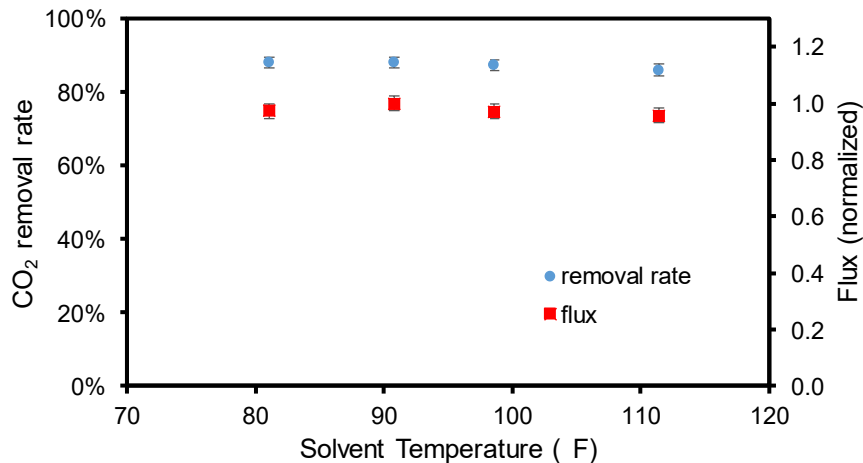


**Figure 22.** Normalized CO<sub>2</sub> flux and removal rate of the flue gas at 118 °F as a function of solvent temperature. Gas side: 12% CO<sub>2</sub> concentration and 13 psig feed pressure; liquid side: 15 psig inlet pressure and 5.4 L/min flow rate.

### 5.2.5. Carbon dioxide capture rate

Figure 23 shows that the CO<sub>2</sub> flux decreased with an increasing CO<sub>2</sub> capture rate. To achieve a high CO<sub>2</sub> capture rate, the total flue gas flow rate to the module needed to be decreased. By treating less flue gas, a very high capture rate could be achieved. However, this resulted in a lower flux, as there was less total CO<sub>2</sub> being introduced to the membrane.

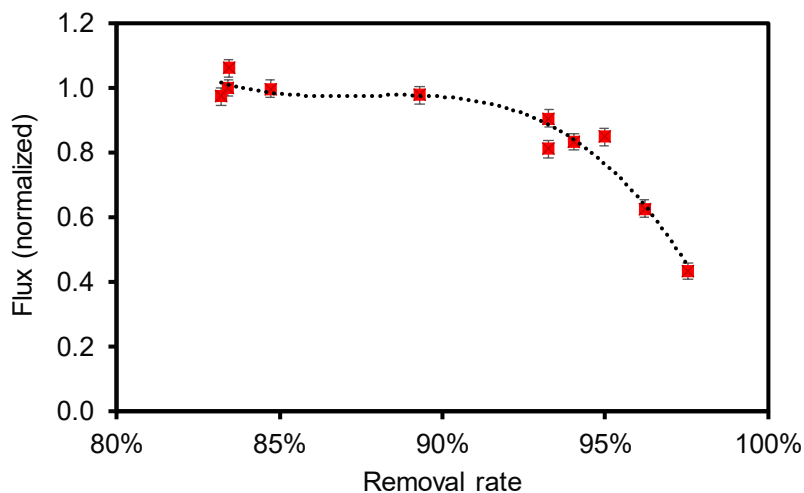


**Figure 23.** Normalized CO<sub>2</sub> flux for a flue gas at 109 °F as a function of CO<sub>2</sub> removal rate. Gas side: 12% CO<sub>2</sub> concentration and 11.3 psig feed pressure; liquid side: 14.5 psig inlet pressure and 5.5 L/min flow rate.

Based on the parametric testing, the operating conditions for full-scale (28 modules) and 2-month continuous testing were determined.

Continuous testing with 28 membrane modules, however, did not match the single module results; the CO<sub>2</sub> capture performance declined with time. Quantitative analysis as well as inspection and measurements of the spent modules were conducted to investigate the potential causes. The major issue identified was the tubesheet leaks from patch points and potentially from fiber/epoxy separation due to non-uniform bonding. Corrective actions addressing cartridge shortcomings have been developed and incorporated into the fabrication of four membrane bundles. The resulting four membranes were tested at NCCC. The results indicate that the decline trends for CO<sub>2</sub> removal rate and CO<sub>2</sub> removal flux were nearly identical to those of the previous tests conducted in 2018 and 2021. Inspection and property measurement of the spent modules are underway to identify approaches for further membrane improvement.

### 5.3. Long-term tests

#### 5.3.1. 2018's tests with 28 modules

Figure 24 shows the CO<sub>2</sub> capture rate throughout the 428 hours of testing. Initially, all 28 modules were online, and all process conditions were held constant. At 133 h, four clusters were blocked off, and the total number of modules online was decreased to 12. As shown, the performance declined with time.

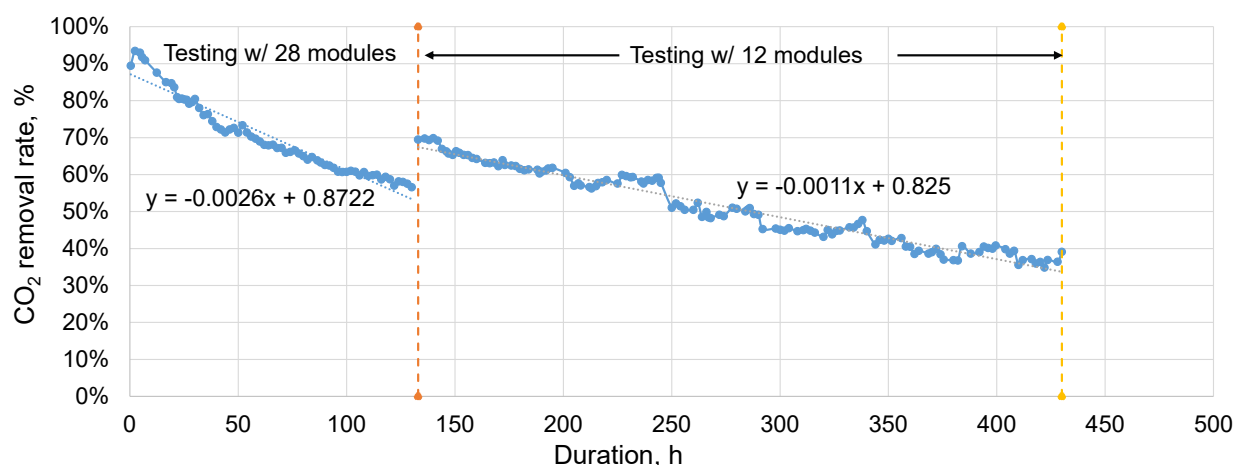


**Figure 24.** CO<sub>2</sub> removal rate as a function of time during 2018's tests.

The post-test inspection found some white, powdery material and rust particles on the flue gas inlet side of the membrane (Figure 25). Analysis indicated the white material is calcium sulfate (possibly from the FGD system) or sodium sulfate (possibly from NCCC's pre-scrubber system). Further quantitative analysis indicated three potential causes of the decline in performance: 1) contaminants (powder and rust particles); 2) vapor condensation in fiber bores; and 3) capillary condensation of vapor in

PEEK pores. After discussing with DOE, the decision was made to resolve the issue of contaminants (powder and rust particles) first.



**Figure 25.** Photograph of the flue gas inlet side of the membrane after testing.

To protect the membrane, additional flue gas filters and pre-membrane mesh pads were installed. Also, orifice plates were installed to monitor if there was a flow maldistribution issue. With these modifications, seven used membranes and a single new membrane were installed into the A and B clusters and further tests were conducted.

### **5.3.2. 2019's tests with 8 modules (7 used and one new)**

Figure 26 shows the CO<sub>2</sub> capture rate throughout the 626 hours of testing. The stability was improved, especially during the second 313h test. The 2% drop in the capture rate/100h during the second 313h might have been caused by 1) seven spent membranes (containing particles inside) were used in the test, and 2) rust formed in the carbon steel piping between the filters and the membrane header may have contaminated the modules. The following decisions were made:

1. Move forward to fabricate 28 new membrane cartridges;
2. Replace the current carbon steel inlet flue gas piping with stainless steel from the filter housing to the module entrance;
3. Replace the current carbon steel particulate filter housing with a stainless steel housing and install a 1-micron-sized filter; and
4. Install orifice plates on the gas and liquid sides of each membrane to characterize the individual flow characteristics, allowing for a more comprehensive analysis per membrane

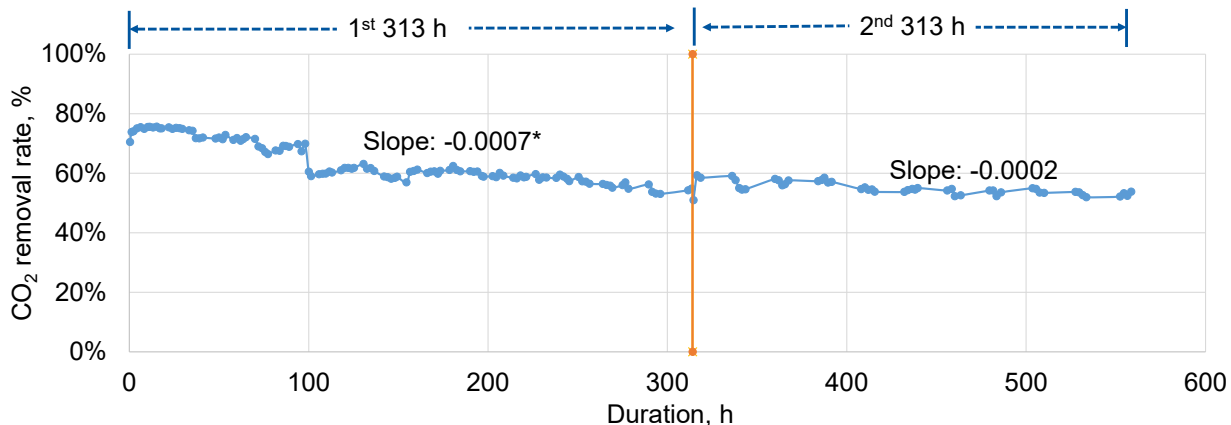


**Figure 26.** CO<sub>2</sub> removal rate as a function of time during 2019's tests with 8 modules.

### 5.3.3. System modification and new membrane preparation after 2019's tests

As planned, piping modifications to the pilot system were completed (Figure 27). Each new orifice plate assembly had an orifice plate with pressure taps and a dedicated differential pressure gauge. The liquid orifice plates were installed on the liquid outlet (rich solvent) with a 0-20 psid differential pressure gauge while the gas inlet orifice plates were installed with a 0-10 psid differential pressure gauge. The flows calculated from these new liquid and gas orifice plates, coupled with the rich amine thermocouples previously installed on each membrane, allowed the performance for each membrane to be determined. New stainless-steel filter housings (Figure 28) were also installed.



**Figure 27.** Modified skid piping.



**Figure 28.** Stainless steel filter housing.

Fabrication of thirty-two (32) 8-inch, commercial-size PEEK HFC cartridges was completed, and 28 of the cartridges were shipped to the NCCC site for further quality assurance testing and pilot-scale performance testing. Initially, each cartridge was leak checked with cyclohexane at ALaS' facility to make sure there were no membrane defects or broken fibers that may have occurred during manufacturing. Any observed defects were repaired. After being dried following the leak checking, the membrane cartridges were further tested at ALaS to measure oxygen and nitrogen permeance. Any broken fibers would have a selectivity of 1.0. Figure 29 shows the average fiber outside diameter (OD) for the 28 cartridges shipped to the NCCC is  $24.3 \pm 0.5$  mil. Figure 30 shows the average fiber inner diameter (ID) for the 28 cartridges is  $16.3 \pm 0.5$  mil. Figure 31 summarizes the oxygen/nitrogen separation factors for the 28 cartridges ( $1.5 \pm 0.1$ ). The membranes were deemed suitable for the pilot-scale CO<sub>2</sub> capture testing.

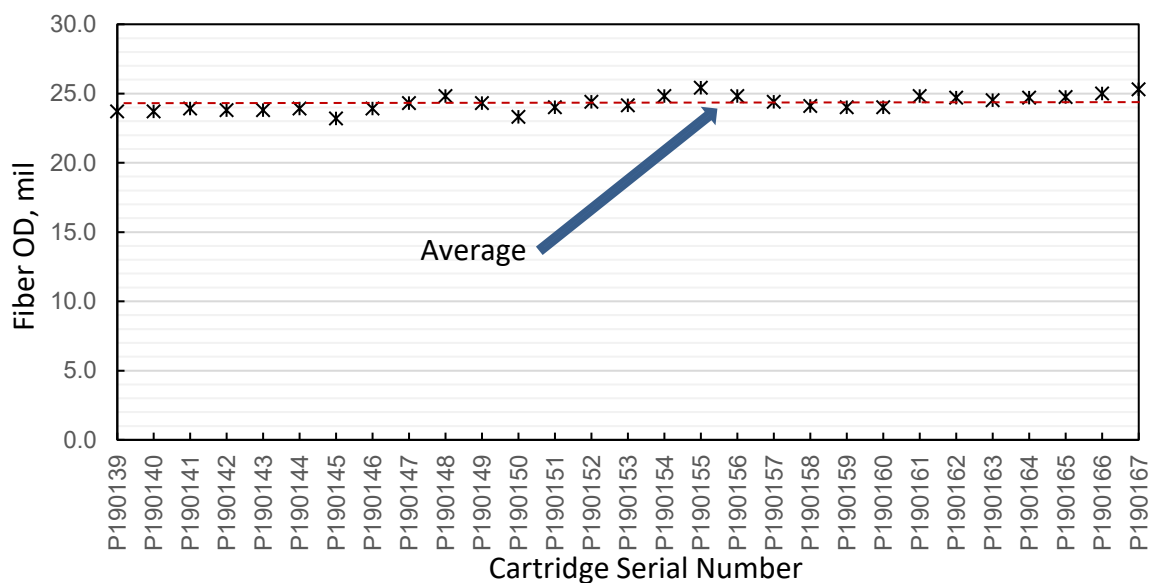


**Figure 29.** Fiber OD for the manufactured cartridges.

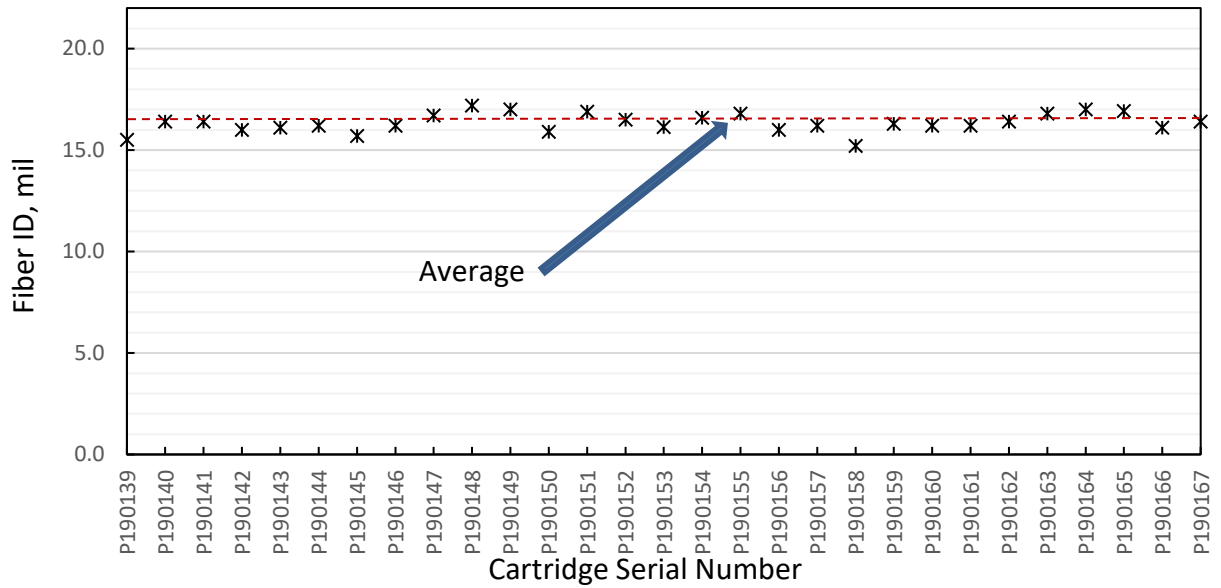


**Figure 30.** Fiber ID for the manufactured cartridges.

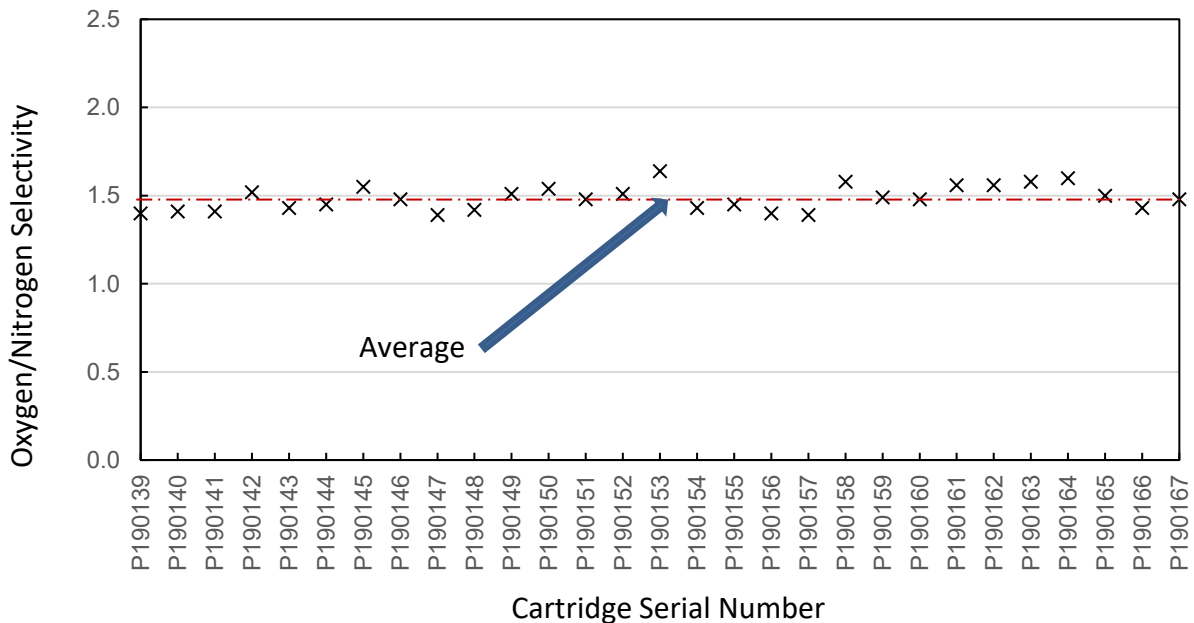


**Figure 31.** Measured cartridge oxygen/nitrogen selectivities.

QC/QA tests were also conducted at NCCC for the new cartridges received from ALaS. Figure 32 shows the membranes track one another. Three membranes were included whose permeances were tested earlier in this project, including data collected from P180001 (spare membrane from the 2018 test campaign), 8PG-4173, and 8PG-4171 (both from previous bench-scale testing). The addition of these membranes shows that the new 8-inch membranes have identical performance compared to 3<sup>rd</sup> generation membranes previously provided for this project.

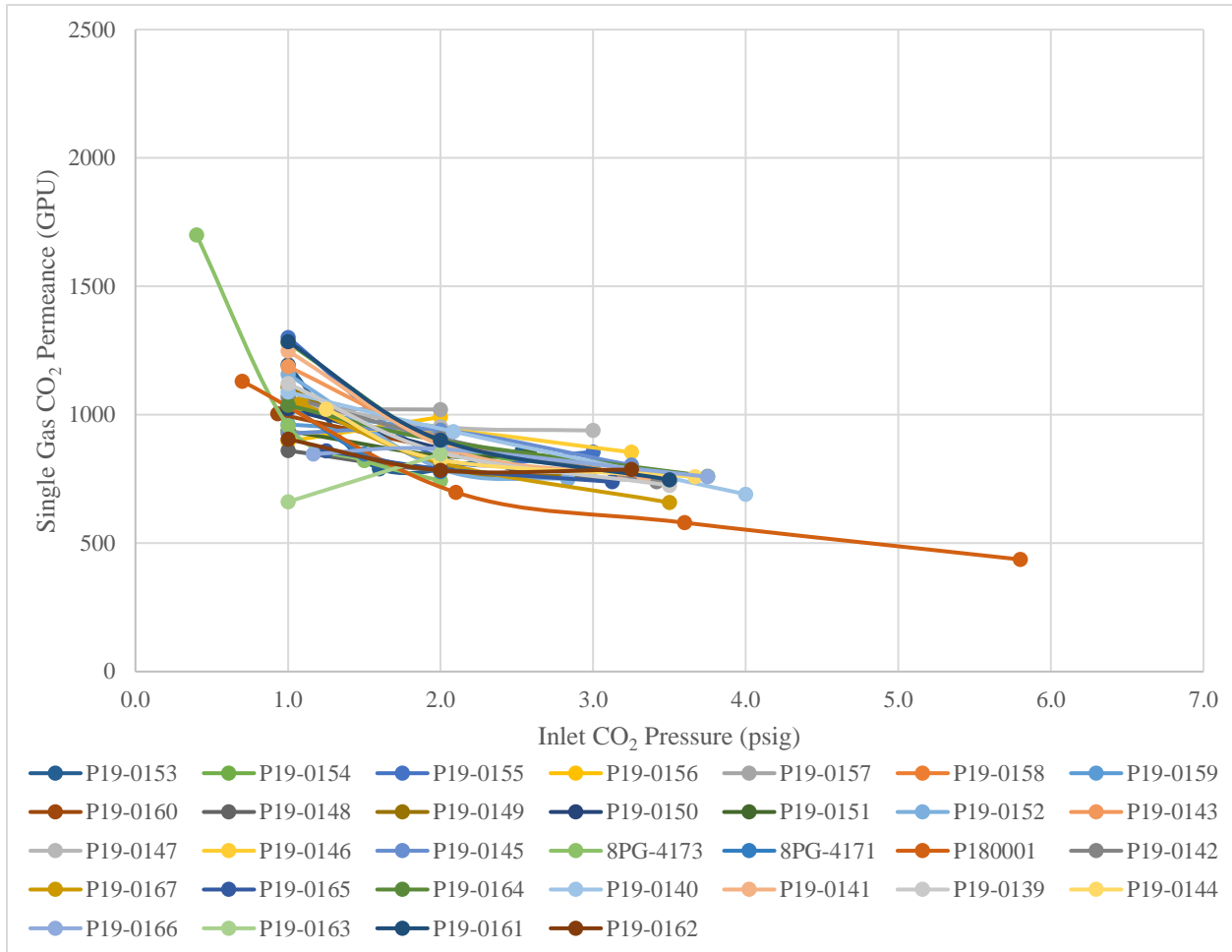


**Figure 32.** Single gas CO<sub>2</sub> permeance versus inlet CO<sub>2</sub> pressure for individual membrane modules.

In addition to single-gas CO<sub>2</sub> permeance, a test was run to look at air permeance through a membrane to compare it to the testing conducted at ALaS. Figure 33 shows the permeance of membrane module P19-0145, using air as the feed gas, for the testing conducted by GTI Energy at the NCCC and oxygen permeance tested by ALaS at their facilities. The recorded permeance for both tests appears nearly identical,

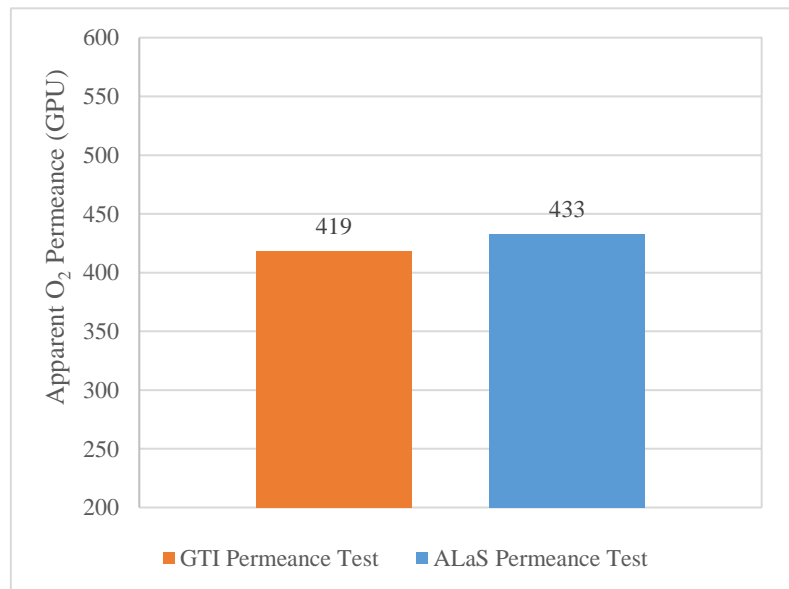


**Figure 33.** Air permeance tested by GTI Energy vs. O<sub>2</sub> permeance tested by ALaS.

indicating good repeatability between the test setup at GTI Energy and ALaS.

#### 5.3.4. 2021's tests with 28 new modules

Due to the impacts of COVID-19 and the unavailability of coal flue gas at NCCC, further testing could not be conducted until early 2021. Once testing resumed, a decline in performance was observed for the first 347 hours during 2021's testing with 28 modules (Figure 34). Inspection suggested that the inlet mesh pads were clean after system improvements, with no visible rust or particulates present on the mesh pads (Figure 35), indicating the issue of particles accumulation on the membranes had been resolved.

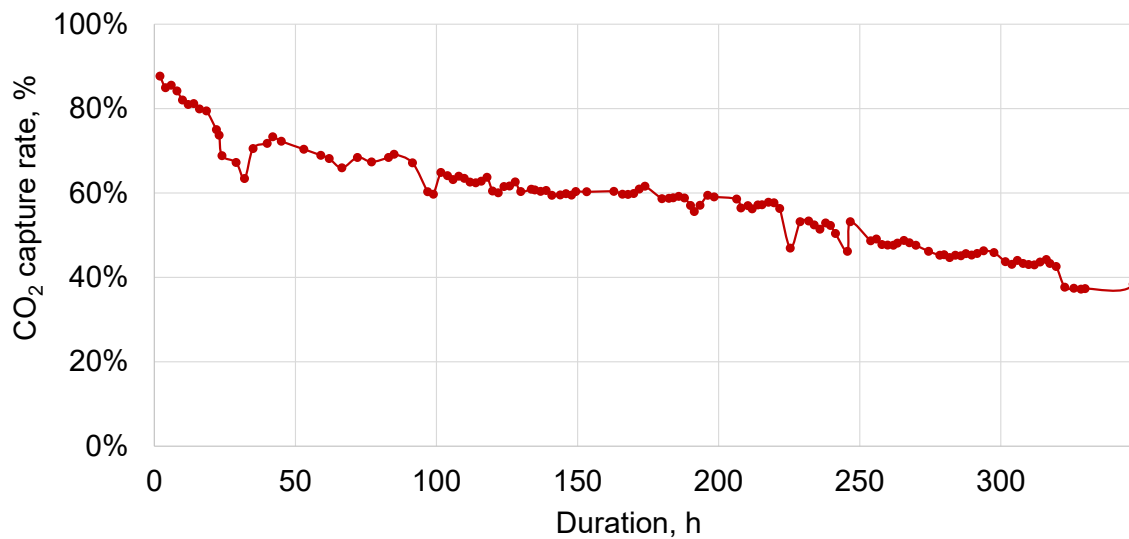


**Figure 34.** 2021's membrane contactor CO<sub>2</sub> capture testing results with 28 fresh modules.



**Figure 35.** A used mesh pad from the top surface of a membrane after 2021's testing.

Two approaches were attempted to recover the membrane performance: 1) a water wash followed by air dry; and 2) an air dry without a water wash. For the first approach (water wash followed by air dry), the following steps were included:

1. Drain liquid from the shell side of the membrane;
2. Remove the inlet mesh pad;
3. Connect demineralized water to the gas inlet, allow water to flow down to the gas outlet (Figure 36);
4. Connect instrument air to the gas inlet, purge fibers with air; and
5. Replace gas inlet mesh pad, bring membrane back online

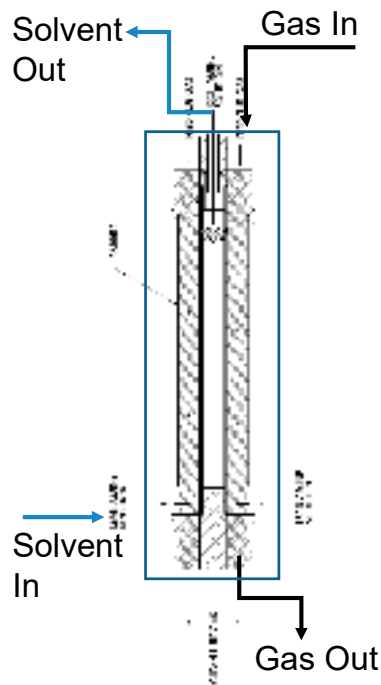


**Figure 36.** Membrane module connections.

For the second approach (air dry without water wash), only steps 1, 2, 4, and 5 were applied.

Approaches 1 and 2 were employed for Cluster F and G modules respectively. As shown in Figure 37, air purge alone was not sufficient in recovering performance. In contrast, a water wash followed by an air purge can recover the performance but didn't resolve the continual decline issue. The effects of operating conditions (data not shown here) such as feed flue gas temperature and DP between liquid and gas sides were also investigated. The change in these conditions did not improve stability.

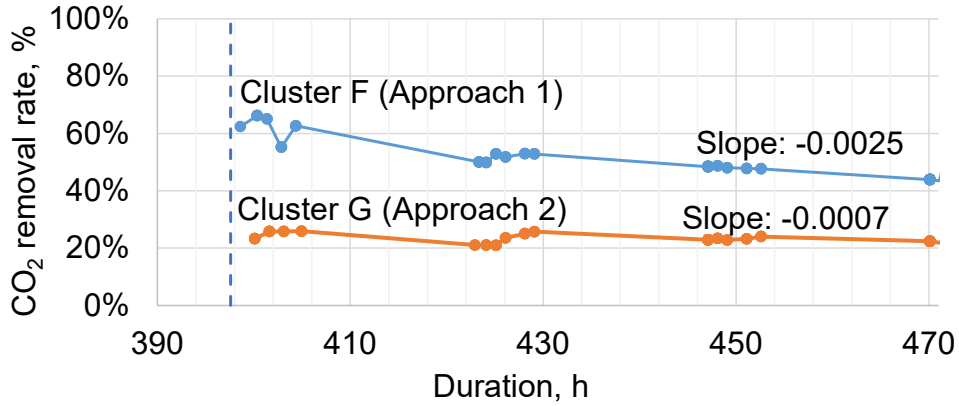


**Figure 37.** Performances of Cluster F and G modules after different approaches were employed.

### 5.3.5. Quantitative analysis, module inspection, and measurements after 2021's tests

#### 5.3.5.1. Quantitative analysis

Quantitative analysis was conducted after the tests. Possible causes of performance degradation and mitigation/actions required to resolve the issues are given in Table 4.

**Table 4.** Possible Causes of performance degradation and mitigation/action required to resolve.

Cause #	Explanation	Sub-cause #	Explanation	Mitigation/Action Required to Resolve	Resolved?
1	Contaminants in the flue gas	A	Solids (rust and white powder) were observed on inlet tubesheets and in bores	Replaced piping with stainless steel, installed filter, mesh pads in 2020	Yes
		B	Within bore or pore, water vapor condenses, blocking CO <sub>2</sub> passage	Reduced flue gas dewpoint with no effect on degradation. Liquid found in the bore is consistent with amine, NOT flue gas	Yes, verified to not be the cause
2	Liquid was observed from the bore side drain with amine concentration close to solvent	A	Poor membrane potting into epoxy tubesheet provides a path	ALaS developed an infusion technique to eliminate leak path in 2016	Yes, verified to not be the cause
		B	Broken fibers during operations provide a path for amine to get into the top tubesheet and into the bores	Perform solvent permeation test at ΔP of 1-10 psi, single gas permeance tests, and cyclohexane tests	Need action

		C	Defects of the membrane super-hydrophobic layer coating during handling or operation	SEM and other characterizations, single gas permeation testing, solvent permeation testing, cyclohexane testing on used modules	Need action
		D	Membrane hydrophobicity changes (especially surface contact angle) after long-term contact with liquid	ALaS: measure contact angle as a function of time in the presence of solvent	Need action
		E	Vapor phase permeation of the solvent through the membrane and then condensation in the pores and in the bore	GTI: V-L-E data for amine solution, amine and water permeances to calculate the amine concentration of the condensed liquid; ALaS: prepare PEEK with pores > 50 nm (current pores have an average size of 13-16 nm).	Need action

### 5.3.5.2. Characterization and analyses of returned NCCC membrane cartridges

#### 5.3.5.2.1. Membrane cartridge return and re-qualification testing

Four membrane cartridges (P190139, P190144, P190165, and P190166) were returned to the Air Liquide Advanced Separations (ALaS) facility in Woburn MA (ALaS – Woburn) from the NCCC test site for analyses to identify the potential causes for the CO<sub>2</sub> absorption performance degradation during the field operation. Initial inspection of P190166 revealed a severe crack in the neat epoxy section of the tubesheet (Figure 38). The crack traversed the O-ring groove, rendering the O-ring ineffectiveness in sealing the cartridge in the shell. Cartridge P190166 was replaced with P190167 for the analysis, including bundle level requalification using the standard manufacturing quality control (QC) test protocol. The crack occurred during removal from the membrane housing.



**Figure 38.** Cracked tubesheet of cartridge P190166.

Liquid removal from the returned cartridges proved far more difficult than anticipated. Cartridge weight was tracked for over a month with no evidence of weight stabilization. Active dry air purge was employed to accelerate drying. QC testing with O<sub>2</sub> and N<sub>2</sub> was repeated over a 16-day period to achieve stable gas permeation results. These data were averaged and are shown as 9/20-10/06 (avg) in Table 5.

**Table 5.** Requalification of returned NCCC membrane cartridges.

Date	P190139 O <sub>2</sub> Perm	P190139 (O <sub>2</sub> /N <sub>2</sub> )	P190144 O <sub>2</sub> Perm	P190144 (O <sub>2</sub> /N <sub>2</sub> )	P190165 O <sub>2</sub> Perm	P190165 (O <sub>2</sub> /N <sub>2</sub> )	P190167 O <sub>2</sub> Perm	P190167 (O <sub>2</sub> /N <sub>2</sub> )
12/14/2019 "as-made"	1.0	1.4	0.9	1.5	1.2	1.5	0.8	1.5
9/20-10/06 (avg)	1.1	1.9	1.1	2.0	1.0	1.7	0.7	1.5
% change from "as-made"	10	32	20	33	-20	13	-15	8.7

\*Normalized Permeance used for all data

A clear pattern emerged for O<sub>2</sub>/N<sub>2</sub> selectivity (Table 5). In all cases, selectivity increased significantly (7%-32%). During the manufacture of membranes, it is possible to trade selectivity for productivity. For this application, cartridge productivity was lower than desired, and selectivity is relatively unimportant, as long as the loss in selectivity is not due to a defect in the membrane allowing the viscous flow of gas or liquid flow into the gas phase. These cartridges were intentionally manufactured for high permeance and lower selectivity. For the contactor, the membrane acts as a physical barrier, allowing differential pressures across the membrane that are potentially orders of magnitude greater than that allowed by surface tension effects, without permitting liquid intrusion into the porous substructure. It was jointly decided to produce high productivity modules at the expense of selectivity.

The service life of these modules appears to have caused aging or "tightening" of the membrane structure. This is not uncommon. The typical target selectivity for this product is an O<sub>2</sub>/N<sub>2</sub> selectivity of 2. The returned cartridges approach this value.

Typically, the increase in selectivity through aging is accompanied by a decrease in productivity. This is not borne out by the data. Two cartridges (P190139 and P190144) have increased permeance while two cartridges (P190165 and P190167) have decreased permeance upon retesting after the field test.

### 5.3.5.2.2. Cartridge autopsy and fiber characterization

The next step in the analysis was cartridge autopsy. In this work, fiber was systematically removed in layers with accompanying photo documentation. Fiber samples were collected for mini-permeator permselectivity testing and analytical work.

Cartridge P190166 was the first bundle to be autopsied. This cartridge could not be tested upon receipt due to the large tubesheet crack across the O-ring groove. Figure 39 shows layers of fiber from the OD of the fiber mass to the ID of the fiber mass as the autopsy progressed. The results are unusual, unexpected, and difficult to explain. The

OD of the bundle, just inside the elastic sock (employed to protect the fiber from handling during module production), appears reasonably normal. The majority of the fibers are light, with minimal if any discoloration. There are 4 brown fibers present running the length of the cartridge. Moving to the midpoint of the fiber mass, a heavily discolored area of the fiber is revealed. There are fibers of normal color intertwined with intense brown-colored fiber. At the fiber mass ID, there is a mix of fiber colors, but none with the color intensity of the fiber mass midpoint. Fiber samples collected from each region as described above were tested for O<sub>2</sub>/N<sub>2</sub> permeance and selectivity.

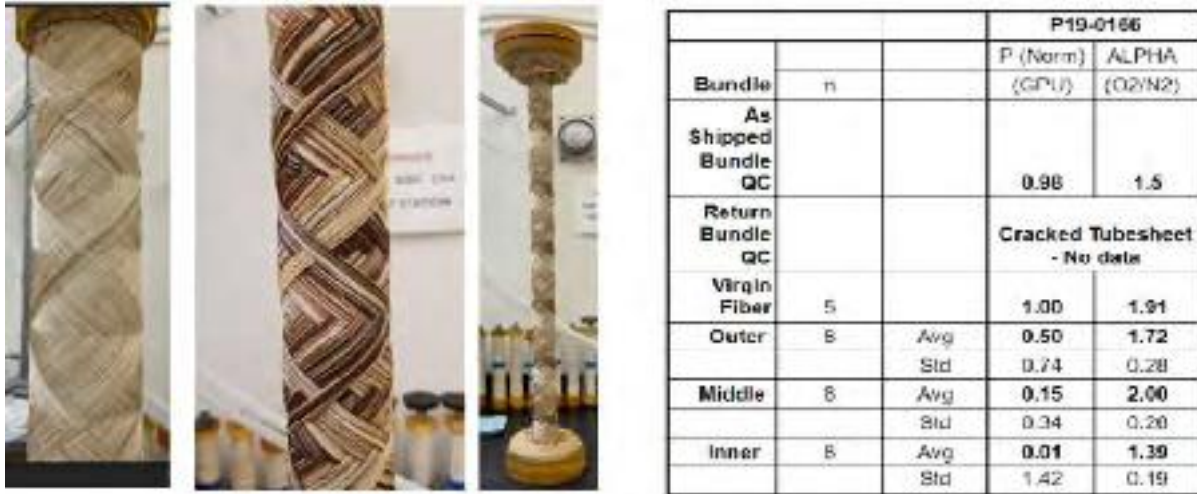


**Figure 39.** Autopsy pictures of Bundle P190166 (cracked tubesheet).

A wide range of permeance and selectivity was measured for the three layers of fiber. For P190166, permeance was affected to a greater degree than selectivity. Outer layer fiber was 50% as permeable as virgin fiber. The middle-layer permeance was 15% of virgin fiber, and the inner-layer fiber permeance was only 2% of virgin fiber. The fiber remained selective, with outer and mid layers showing moderate effects. The inner layer lost 27% of virgin fiber selectivity. Separate mini-permeators were fabricated to determine permselectivity differences between discolored brown fiber and white fiber (Table 6). It is interesting to note that the entire length of the fiber is either white or uniformly discolored. No fiber is half white and half brown.

**Table 6.** Permselectivity comparison of white and discolored fiber from P190166.

Module P19-166				
Location in		P (Norm) (GPU)	ALPHA (O <sub>2</sub> /N <sub>2</sub> )	
Bundle	n			
Outer-White	5	Avg	0.58	1.87
		Std	0.72	0.33
Outer-brown	2	Avg	0.31	1.83
		Std	0.48	0.05

Module P19-166				
Location in		P (Norm) (GPU)	ALPHA (O <sub>2</sub> /N <sub>2</sub> )	
Bundle	n			
Inner-White	5	Avg	0.02	1.49
		Std	1.2	0.14
Inner-Brown	2	Avg	0.002	1.29
		Std	0.4	0.19

Both the outer and inner brown fiber had lower permeance than the white fiber. The brown inner fiber was nearly impermeable yet retained some selectivity.

P190166 (cracked tubesheet) showed a far greater impact from contamination than all other cartridges. It also showed the largest degree of contamination. This is either consistent with this cartridge having the highest leak rate, or it suggests the operation of the cartridge with the crack present. Either of these issues would lead to gross contamination by the amine solution.

### 5.3.5.2.3. Analysis of brown fiber

The difference between the brown and white fiber is striking (see Figure 40). FTIR and ATR-FTIR were performed on the discolored fiber. It was determined that isopropyl alcohol (IPA) could extract color from the **chopped** fiber. Immersion of unchopped brown fiber with the ends of the fiber outside of the IPA bath extracted no color. It was deduced that the origin of the color was extracted from the fiber bore.



**Figure 40.** Close-up photographs of discolored fiber.

As shown in Figure 41, FTIR of the IPA extract is compared to the reference spectrum for MDEA and two representative amine /amide compounds (2,2-Diaminomalonamide, L-2-Amino-1-Propanol, Bis-(2-hydroxyethyl)methylamine, and Di(2-hydroxyethyl)methyl amine). The FTIR traces are very similar. The presence of the extra ~1650 and ~1590 bands indicates that additional carboxylate ions may be present which suggests MDEA degradation products.

Contact transfer ATR-FTIR from the fiber OD surface detected silicone oil and low levels of degraded MDEA. No information was obtained from the fiber ID due to the inability to make crystal contact with the fiber.

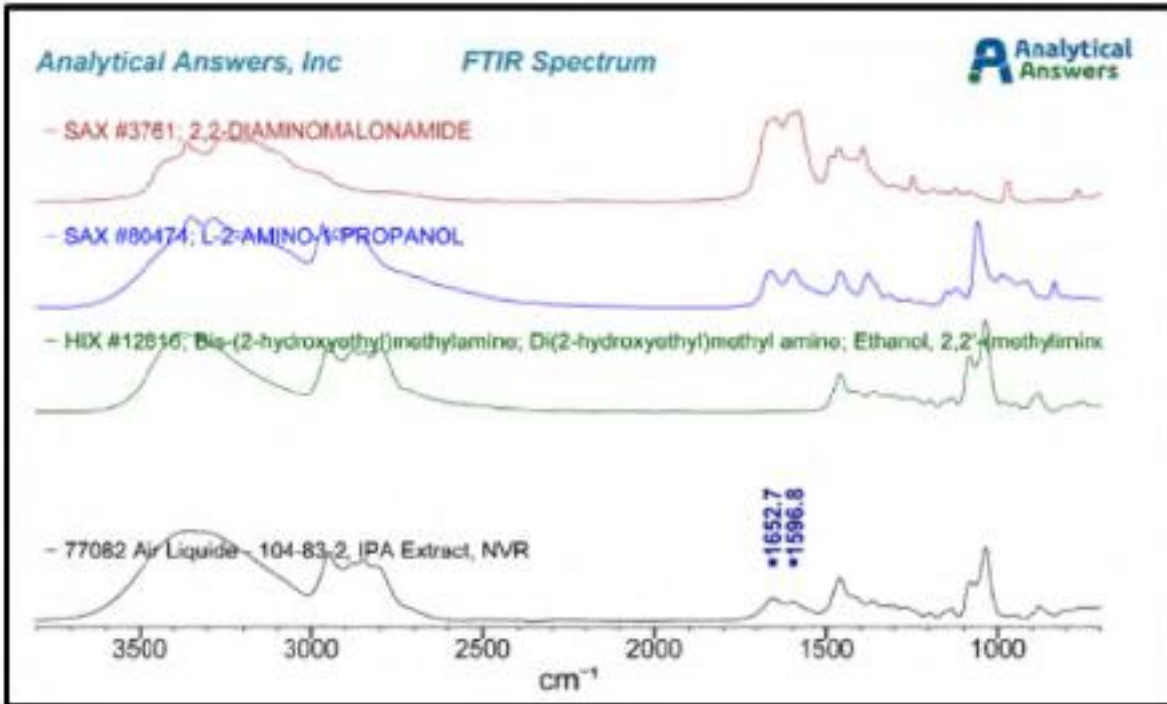


**Figure 41.** FTIR analysis of IPA extractant from chopped brown fiber.

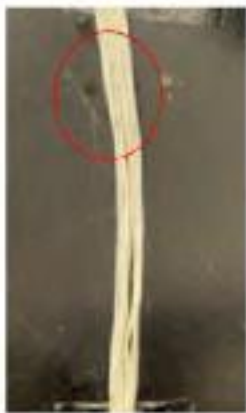
**5.3.5.2.4. Superhydrophobic Layer Integrity as evidenced by surface energy**

Contact angle measurements on a curved surface, such as the OD of a fiber, are complex. To determine if the superhydrophobic layer was altered in service, a simple experiment was devised to estimate the surface energy of the fiber OD and compare virgin fiber to returned fiber.

Multiple fibers (white and discolored brown) were laid parallel to each other and taped in place. Drops of the liquids in Table 7 were placed on the fiber using a syringe. If the surface of the fiber had a surface energy greater than the surface tension of the liquid, the liquid would spread. If the surface energy of the fiber was lower than the surface tension of the liquid, the liquid would bead on the surface. Results are shown in Figure 42.

**Table 7.** Surface tension of selected liquids.

Liquid	Surface Tension (dyne/cm)
Water	72.8
Ethylene Glycol	47.7
Dichloroethane	33.3

Liquid	Virgin Fiber	P190139 White	P190139 Brown
Water 72.8 dynes/cm			
Ethylene glycol 47.7 dynes/cm			
Dichloroethane 33.3 dynes/cm			

**Figure 42.** Surface tension estimates of virgin, white, and discolored fiber.

The red circles in Figure 42 highlight the liquid addition. Beads were observed with the addition of water (72.8 dyne/cm) and ethylene glycol (47.7 dyne/cm). Neither of the liquids wetted any of the fibers. There was no evidence of bead formation with Dichloroethane (33.3 dyne/cm) addition. Dichloroethane wetted all fibers. This work was repeated with 10 samples yielding the same result.

These experiments indicate that the surface energy of all fibers lies between 33.3 dyne/cm and 47.7 dyne/cm. This conclusion applies to the virgin, white-returned fiber, and brown discolored fiber, suggesting the fiber surface (in contact with the absorbing liquid) is the same for all fibers and is hydrophobic. This result is also consistent with the

FTIR studies and the observation that brown discoloration could only be extracted from chopped fiber and not lengths of fiber with ends above the liquid level.

### 5.3.5.2.5. Cartridge autopsy and fiber characterization after dye/leak testing

Cartridges were dye/leak tested in addition to autopsy and mini permeator testing. 0.1 wt.% crystal violet was dissolved in a 10% IPA/90% water solution. The alcohol-water mix closely matches the surface tension of the amine solution previously tested at NCCC. The cartridges were placed in a housing and the dye solution was applied at pressure up to 5 psig. The solution was recirculated through the vessel for 20 minutes. After the dye test, a 1/8" wafer was cut from the end of the tubesheet to reveal a clean tubesheet surface.

Tubesheet leaks were identified for all cartridges. The pressure was reduced to <1 psig for P109167 due to the high leak rate. Most leaks originated from epoxy repair on the tubesheet to patch point leaks in the tubesheet face. None of the cartridges showed evidence of dye uptake by the fiber. This suggests that the superhydrophobic surface coating is intact - a point also reinforced in the previous section of this report. Details for the individual cartridges are as follows:

Cartridge P190139 contained minimal brown fibers and like all other cartridges, no blue-stained fiber. The bundle-level QC performance indicated an increase in permeance and selectivity. Individual testing on the three layers of fiber yielded similar performance. Permeators made from the three layers had permeance higher than that of virgin fiber and selectivity very similar to that of the virgin fiber (Figure 43).



**Figure 43.** Cartridge P190139 - autopsy pictures and fiber performance.

The tubesheet face of P190139 showed two major leaks. Both were associated with patching of leak points from manufacturing as evidenced by the circular plugs (Figure 44). This is unexpected and unusual.



**Figure 44.** Dye stains originating from tubesheet patches.

This is difficult to explain in light of the re-QC data indicating only a slight increase in O<sub>2</sub> permeance and a significant increase in selectivity from 1.4 to 1.9.

Further inspection of the tubesheet wafer shows evidence of white debris in the bore of the fiber as well as tinges of rust color (Figure 45). The rust color could also be the result of amine contamination due to the tubesheet leak. The white powder in the fiber bore indicates that Cause 1A (Table 4) is not fully addressed.

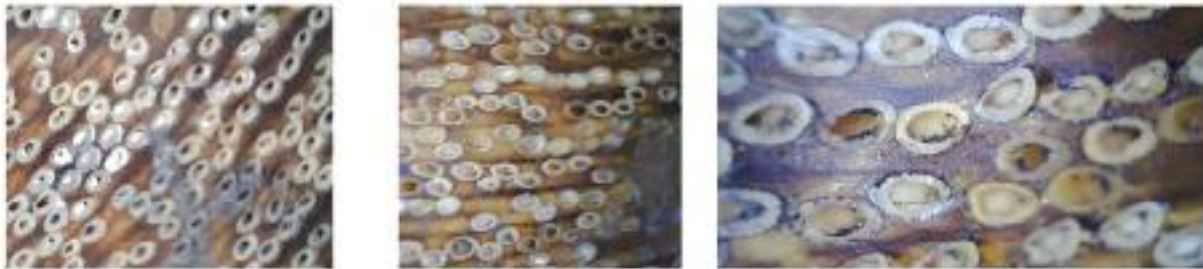


**Figure 45.** Photographic evidence of debris in the fiber bore in P190139.

A few brown fibers were collected from the outer layer of P190139 and the gas permselectivity was measured and compared to the white fibers (Table 8). The impact of the contamination is far less severe than that observed for bundle P190166. Productivity and selectivity are higher than that for the as-shipped cartridge. That is probably due to the low level of contamination compared to P190166.

**Table 8.** Comparison of permselectivity for OD layer of P90139.

Module P19-139				
Location in			P (Norm)	ALPI A
Bundle	n		(GPU)	(O <sub>2</sub> /N <sub>2</sub> )
Outer-White	4	Avg	1.7	1.81
		Std	0.29	0.04
Outer-Brown	4	Avg	1.1	1.98
		Std	0.23	0.11

Autopsy and analysis of cartridge P190144 yielded results very similar to P190139 (Figure 46). There are very few brown discolored fibers. Again, entire fiber lengths are either white or discolored. Bundle-level QC results of the returned cartridge are higher than the as-shipped QC results. Fiber level performance indicates high O<sub>2</sub> permeance and O<sub>2</sub>/N<sub>2</sub> selectivity slightly lower than virgin fiber. The lower value could be interpreted as a defect in the coating, but the O<sub>2</sub>/N<sub>2</sub> selectivity is higher than the as-shipped bundle and no fibers were dyed blue.

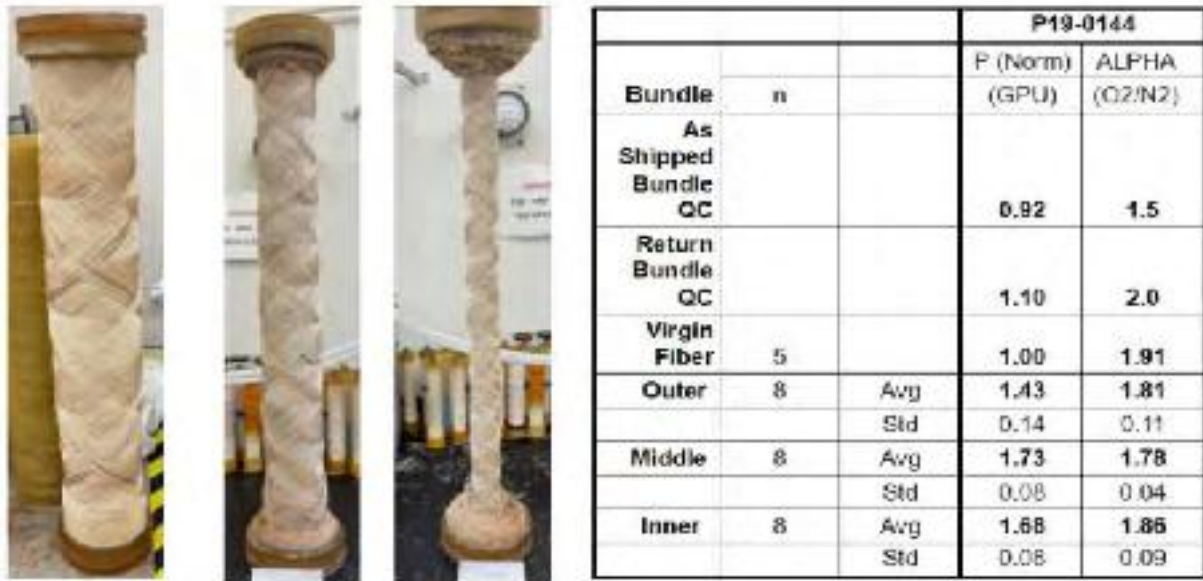


**Figure 46.** Cartridge P190144 - autopsy pictures and fiber performance.

While not captured before, all cartridges contained considerable debris on the shell side of the module. The composition of the debris was not conclusively determined (Figure 47A). The FTIR studies indicate the presence of amine degradation products. The particulate matter has a color similar to rust. Figure 47B again shows dye trails sourced by leaks at the tubesheet patch point. The leaks were not as severe for P190144. Figure 47C shows a close-up of fiber with white powder debris in the bore of the feed-end tubesheet.

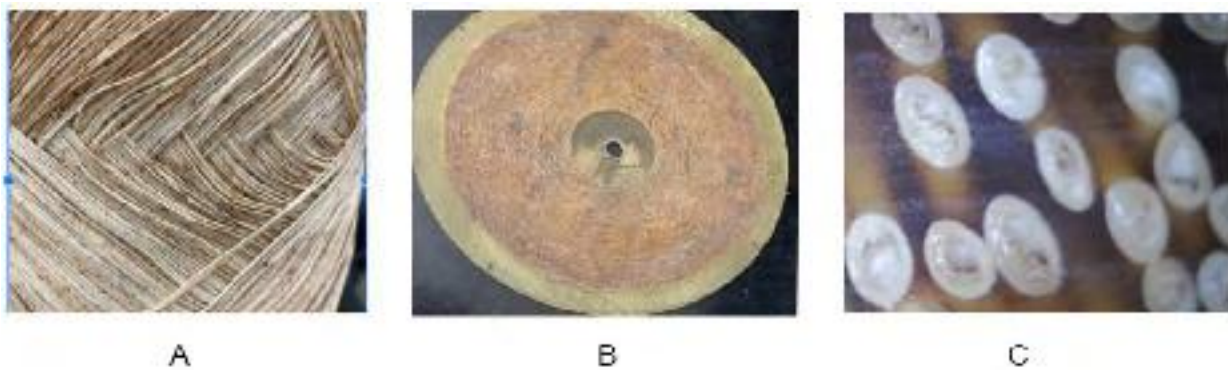


**Figure 47.** Tubesheet leak and debris on cartridge P190144.

P1900165 deviated from the previous bundles (Figure 48). The bundle OD exhibited a few very dark brown fibers. The mid layer and remainder of the fiber mass had a uniform discoloration. QC data indicated that this was initially a high permeance cartridge that decreased in permeance, unlike P190139 and P190144. This cartridge also had the second highest tubesheet leak rate as qualitatively measured through dye testing. On the fiber level, O<sub>2</sub> permeance is increased relative to virgin fiber but O<sub>2</sub>/N<sub>2</sub> selectivity is slightly decreased.



**Figure 48.** Cartridge P190165- autopsy pictures and fiber performance.

Close examination of the tubesheet showed once again debris in the fiber bore (Figure 49). There is also delamination between the fiber and epoxy in the left image of figure 49. Crystal violet dye is on the face of the fiber. It is uncertain if the dye is surface dye or dye that penetrated the tubesheet. Epoxy above and below the blue-stained fiber appears amber.

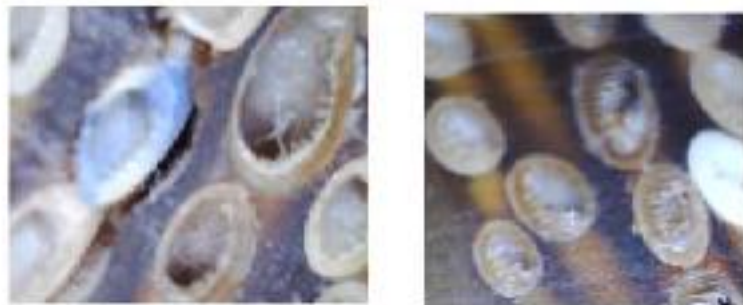


**Figure 49.** Cartridge P190165 tubesheet - white debris in fiber bore, delamination, and crystal violet dye.

P190167 had the highest leak rate during the dye test (Figure 44). Note that P190166 could not be dye tested due to the cracked tubesheet. This bundle also showed the highest incidence of discolored fiber other than P190166. The mid-layer

picture closely resembles the pattern shown in P190166. The discolored fiber is evident in all three layers. Discoloration in this cartridge more closely resembled the mosaic pattern of P190165 than the previous bundles. Bundle-level QC measurements show the  $O_2/N_2$  selectivity is increased slightly from 1.5 to 1.6, the lowest increase of any cartridge. Fiber level performance is the lowest of the returned bundles.  $O_2$  permeance is slightly increased and  $O_2/N_2$  selectivity is depressed relative to the other returned cartridge similarly to P190165.



**Figure 50.** Cartridge P190167- autopsy pictures and fiber performance.

Large leaks observed at the top of the tubesheet face are consistent with the observation of a high dye leak rate. A closer inspection of the face showed fiber/epoxy separation. There is some uncertainty if this is a leak path as the epoxy in the crevice is amber and not stained blue. The separation could result from the 1/8" cut from the tubesheet face. Notice the brown discolored fiber (Figure 51C) with no debris, clear separation, and no debris which is surrounded by white fiber with partially occluded bores.

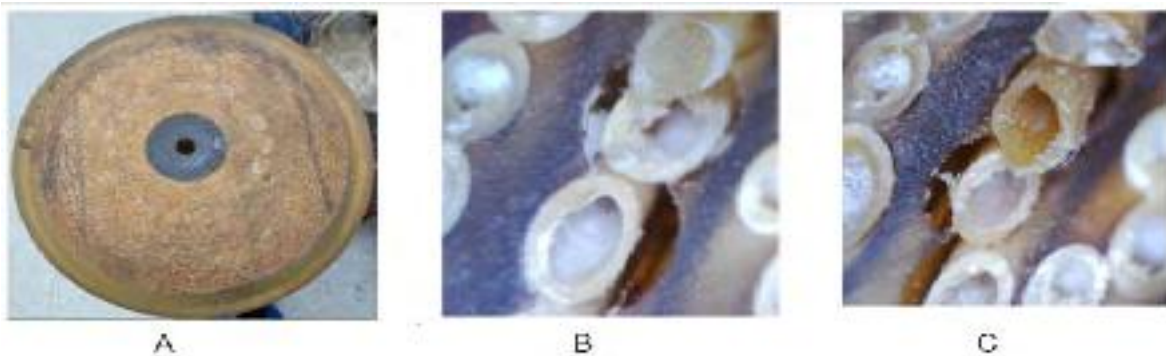


**Figure 51.** Cartridge P190167- autopsy pictures and fiber performance.

### 5.3.5.2.6. Tubesheet and fiber adhesion analysis

The tubesheets of P190165 and P190167 showed evidence of fiber separation from the epoxy. Destructive tubesheet testing was undertaken to evaluate fiber adhesion and tubesheet integrity. Tubesheet wafers were cut from the bundles after dye testing. In addition, tube sheets were cut from the returned bundles. These samples were fractured by mounting in a vice and striking them with a hammer to shear and fracture and/or crushed in a press to rupture. Results from these efforts are similar for all bundles. Sample images of these results are in Figure 52.



**Figure 52.** Fractured tubesheet samples showing delamination of fiber from epoxy.

All fractured tubesheet samples show evidence of non-uniform fiber/epoxy adhesion. The top row of pictures shows fibers pulled away or out from the fiber epoxy matrix on fracture or crushing. However other sections of the fiber are firmly encapsulated by epoxy.

### 5.3.5.3. Discussion of results

Several of the fault tree propositions (Table 4) leading to low CO<sub>2</sub> capture performance can be addressed based on findings from these studies.

1. Cause 1A, Flue Gas Contaminants: "Solids (rust and white powder) observed on inlet tubesheets and in Bores"

To varying degrees, white powder was observed in the fiber bores of all returned cartridges. The vast majority of fibers were not fully occluded. Traces of brown discoloration were observed but attributed to residual amine and amine degradation products.

2. Cause 1B, Flue Gas Contaminants: "Within bore or pore, water vapor condenses, blocking CO<sub>2</sub> passage"

This is a potential cause for the loss in performance but not for the stated reason. In the proposed scenario, low surface tension amine liquid is forced into the bore of some fibers. This can enter the porous substructure and block CO<sub>2</sub> passage. It is also consistent with the water wash-based recovery in performance followed by the gradual decline in performance. It also explains why a simple air purge did little to improve performance. Air purge cannot remove the amine liquid in a short time due to low amine volatility.

3. Cause 2A, Liquid on Bore Side: "Poor Membrane potting into epoxy tubesheet provides a path"

There is very strong evidence of non-uniform adhesion between the fiber & epoxy. There are multiple areas where fiber is pulled from the tubesheet along with sections of fiber fully encased with epoxy. However, all of these fibers are either white or discolored brown with no evidence of crystal violet blue dye. Tubesheet face fiber/epoxy separation was observed for P190165 and P190167. Crystal Blue dye was observed on the tubesheet face, but it is uncertain if the dye originated from a leak through the tubesheet or from a leak from a tubesheet patch.

4. Cause 2B, Liquid on Bore side: "Broken fibers during operation provide a path for amine to get into the top of the tubesheet and into the bores"

There is no evidence to support the presence of broken fibers. The bundle level reQC results showed increased selectivity relative to the "as-made" selectivity.

Mini-permeator testing also indicated an increase in selectivity for the vast majority of samples. The only samples with reduced selectivity were brown fibers with reduced permeance. Broken fibers are typically accompanied by a large increase in permeance, not a decrease. Furthermore, crystal violet blue dye was not observed in the bore of any fibers, when entire cartridges were flooded with the crystal violet dye solution.

5. Cause 2C, Liquid on Bore side: "Defects of the membrane superhydrophobic layer coating during handling or operation"

There is no evidence to support defects in the superhydrophobic coating. Defects in that layer would lead to leaks to the fiber bore. No fibers showed signs of crystal violet blue dye on the surface of any fiber. This is true for both the white and discolored brown fibers. The surface energy estimates support this conclusion due to the similarity of surface energy for virgin, white and brown discolored fiber.

6. Cause 2D, Liquid on Bore side: "Membrane hydrophobicity change (especially surface contact angle) after long term contact with liquid"

The hydrophobicity measurements in this study show all fibers (virgin, returned white, or returned brown) are wet by a fluid of 33.3 dyne/cm. None of the fibers were wet at 47.7 dyne/cm. The surface tension of the amine solution is approximately 45 dyne/cm.

The following scenario is consistent with the information gathered in the RCCA, the observed performance decline in service, and the short-lived bundle recovery protocol (water wash followed by an air dry). During operational service, the amine solution is pressurized above the pressure of the incoming flue gas. Leaks in the top tubesheet of the vertically oriented cartridge allow the amine solution to reach the tubesheet face. Downward flowing gas forces the accumulated amine solution on the top tubesheet down the bore of the fibers. The preferential flow of the amine solution to certain fibers is due to the accumulation and potential occlusion of the fiber bore by the white powdery substance found in all cartridges.

The above scenario appears to be consistent with the visual observations made with full-length brown discolored fibers and no discoloration in others.

This is further supported by the FTIR analysis where the isopropyl alcohol extract from chopped fiber samples substantiates fiber bore contamination by amine and degradation products of amine. Isopropyl alcohol extraction was not possible for long fiber with ends above the liquid level.

The water wash/air dry did temporarily restore CO<sub>2</sub> capture performance but the improvement was short-lived. The water wash removed bore-side amine contamination restoring performance.

Recontamination of the bore with amine solution due to tubesheet leaks caused performance to decline. The ineffectiveness of the air dry-only recovery method is readily explained by the low volatility of the amine solution.

7. Cause 2E, Liquid on Bore side: "Vapor phase permeation of the solvent through the membrane and then condensation in the pores and the bore.

This is possible. However, the effect would be masked by the more dominant issues identified in the root cause analysis.

#### **5.3.5.4. Corrective actions**

From the Root Cause determination efforts described above, corrective actions are being directed to improve CO<sub>2</sub> capture performance and long-term stability of HFMC. Results from the root cause analysis identified no defects or loss in hydrophobicity of the super-hydrophobic coating. The root cause analysis identified tubesheet leaks and non-uniform fiber/epoxy adhesion as the primary issue for absorbent leakage in the membrane contactor. Partial blockage and/or occlusion of the fiber bore due to what appear to be particulates borne by the gas phase is also a potential problem.

The tubesheet patch process was thoroughly reviewed. A change in the epoxy curing procedure was adopted based on experimental results. This change has been incorporated into the work procedures for the HFMC.

Based on the results of these studies, the original procedure to address tubesheet issues was inadequate. This procedure was thoroughly reviewed and followed by a brainstorming session. 2" midi-modules were used for the evaluation and development. Based on midi-module testing, several improvements to the original procedure were developed.

- A more aggressive chemical treatment of the super-hydrophobic fiber mass in the tubesheet region was developed to decrease hydrophobicity and improve adhesion.
- A viscosity modifier was added to the epoxy to ensure full and uniform penetration of the fiber mass with epoxy. Both should increase the uniformity of the epoxy/fiber bond. In addition, a new, two-step potting procedure was developed.
- A proprietary, low durometer, room temperature cure epoxy is added in a second step to improve epoxy fiber bonding and pressure-induced seal in the tubesheet.

Figure 53 shows slices cut away from the improved tubesheets. These corrective actions described above have been incorporated into modified manufacturing work instructions, and four bundles were fabricated for NCCC's testing.

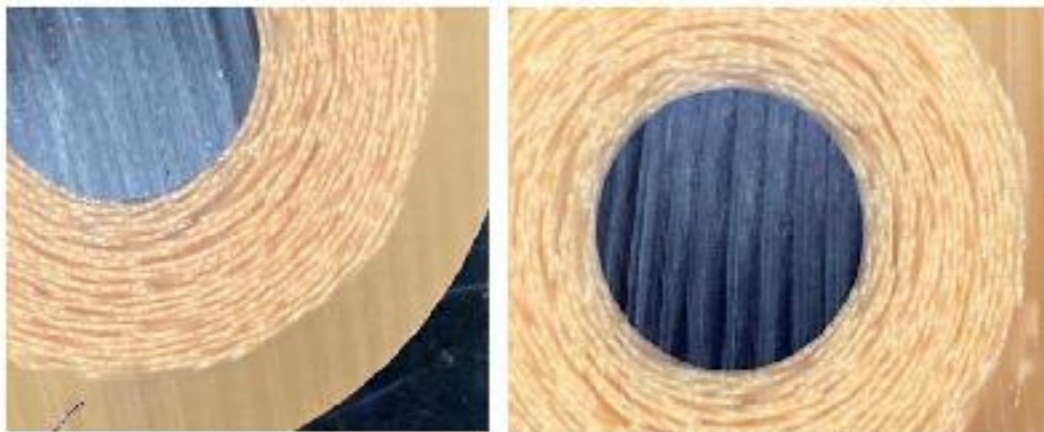


**Figure 53.** Improved super-hydrophobic membrane contactor tubesheet.

#### **5.3.6. 2022's tests with 4 new modules**

The team at ALaS fabricated four 8-inch-diameter membrane modules (P22-0001, P22-0004, P22-0005, and P22-0006) using their updated fabrication process with an improved potting method. In addition to their standard QA/QC, ALaS added a water leak check before shipment. All four membrane modules shipped to the NCCC passed their leak check, proving good adhesion between the epoxy and membrane fiber after fabrication.

GTI Energy personnel traveled to the NCCC, collected the membranes delivered by ALaS, and conducted membrane QA/QC at NCCC. During the QA/QC, the membrane single gas permeance was checked for CO<sub>2</sub> and N<sub>2</sub>. The CO<sub>2</sub> permeances for the four delivered modules, P220001, P220004, P220005, and P220006, were identical to those of the previous membranes. No leaks were observed during the single gas permeation tests.

GTI Energy personnel installed the four membranes into the pilot test unit (Cluster A) and recommissioned the unit. The recommissioning of the unit proceeded without issue. The membranes were then tested for CO<sub>2</sub> capture in gas-liquid contactor mode. The initial testing points showed good CO<sub>2</sub> capture performance. However, over the next 100 hours, the CO<sub>2</sub> removal and CO<sub>2</sub> removal flux continued to decline. Figure 54 shows that the rate of performance decline is similar to the full-scale tests conducted in 2018 and 2021.

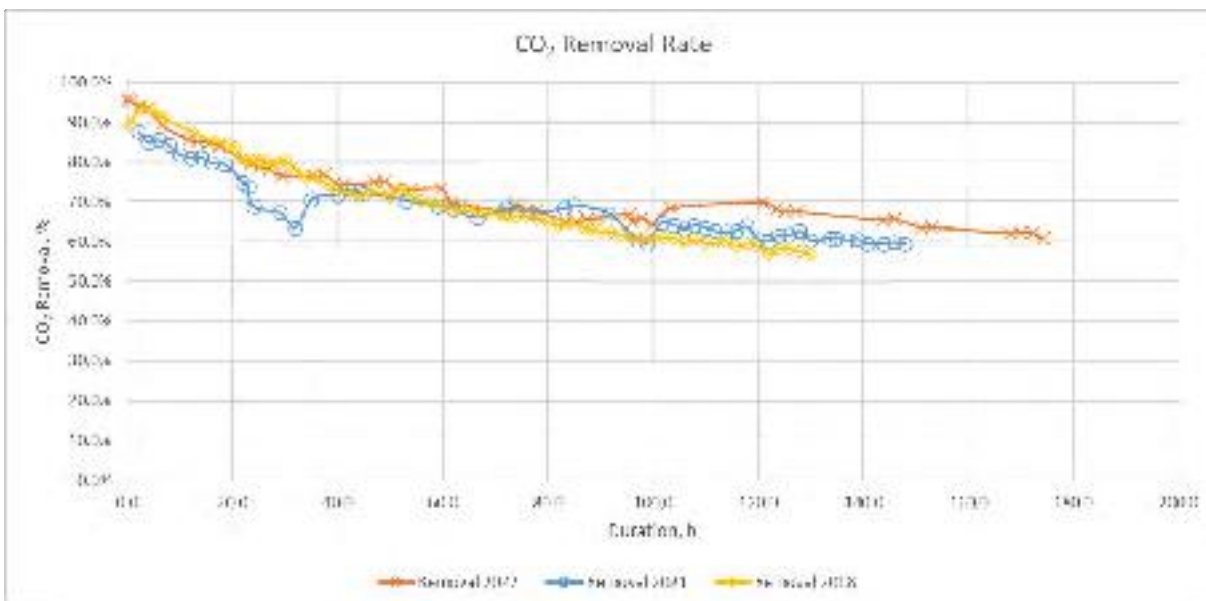


**Figure 54.** CO<sub>2</sub> removal rate as a function of operating time for tests conducted in 2018, 2021, and 2022.

During the test, an amber-colored solution was collected from the gas outlet low point drain. Further measurements indicated the collected solution contained about 20-21 wt.% amine, compared to the 34-35 wt.% amine in the bulk solvent. This indicates some solvent was entering the bore side. At the end of testing, the four membrane modules were washed, dried, and shipped back to ALaS for inspection.

The team at ALaS performed single-gas permeation measurements for the four spent bundles (tested at NCCC). Other than P22-0004, the other bundles show a negligible loss in gas pair (O<sub>2</sub>/N<sub>2</sub>) selectivity. Each bundle was leak tested with an isopropyl alcohol (IPA)/H<sub>2</sub>O mixture to achieve the same surface tension as the amine absorbent. Bundles P22-0001, P22-0005, and P22-0006 had leaks, whereas no leaks were observed for Bundle P22-0004.

## 6. Decommissioning of HFMC System

---

With testing activities concluded, the HFMC system was decommissioned in May 2022. The following equipment items were identified for future carbon capture projects:

- Control hardware
- Control hardware for main 480 VAC distribution panel
- Historian computer and operator control station
- Blower skid and MCC
- Horiba analyzers
- Horiba pre-conditioners
- Particulate filter housings
- Spare parts at the warehouse
- Remaining virgin BASE-OASE Purple solvent.

NCCC personnel assisted GTI Energy with the removal of hazardous materials from the skids for disposal. The skids were removed from the site and scrapped. Figure 55 shows a picture of the cleaned site.

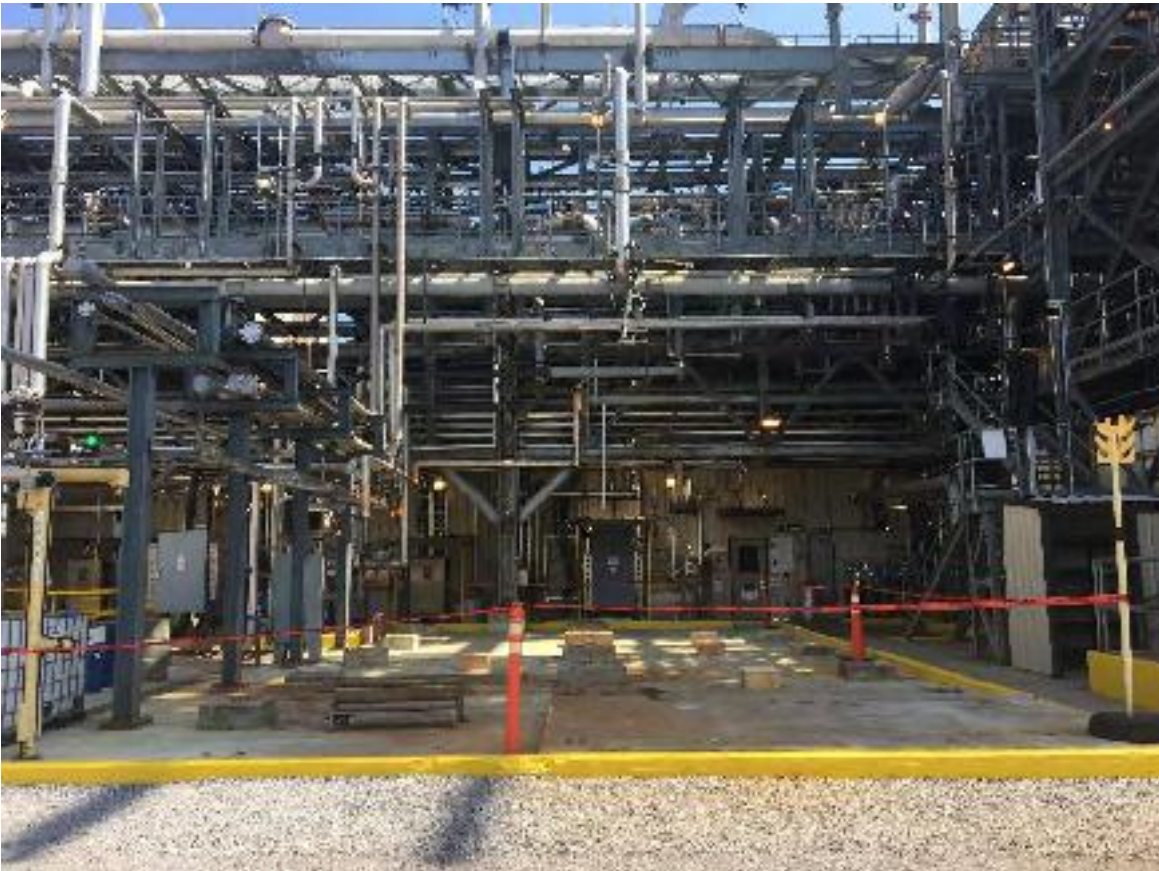


**Figure 55.** A picture of the cleaned site.

## **7. Summary of Lessons Learned and Improvements**

---

Figure 56 summarizes the lessons learned and improvements through the current engineering scale project. Researchers widely study membrane contactor CO<sub>2</sub> capture. This project has advanced the technology to a high TRL level and resolved a number of technical issues (e.g. concentration polarization) that other researchers have not yet dealt with. The project results and publications will be a significant contribution to the literature and other technology developers.

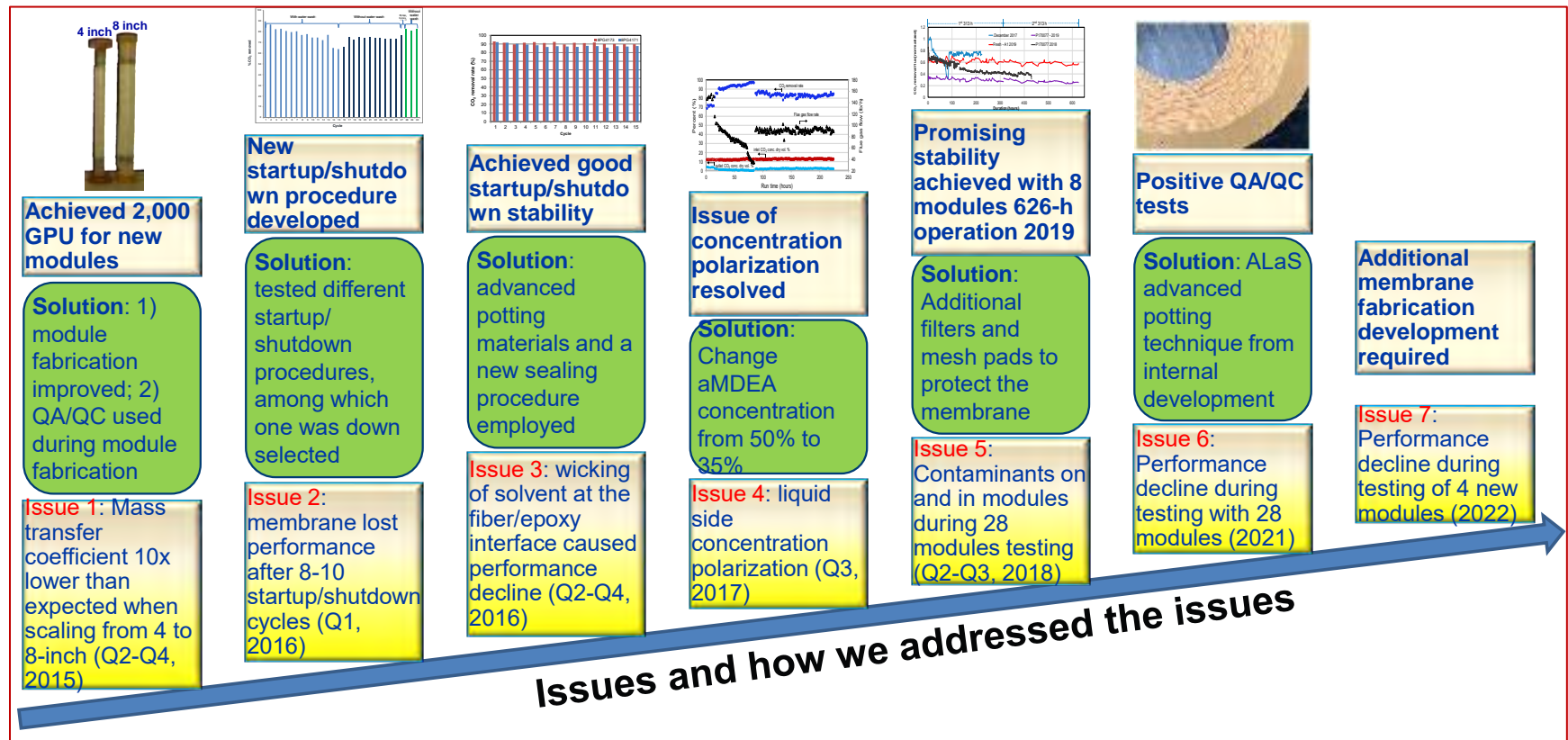


Figure 56. Summary of lessons learned and improvements.

## **8. Summary of Accomplishments and Contribution**

---

- Membranes with intrinsic CO<sub>2</sub> permeance as high as 2,600 GPU were developed, and commercial-sized modules were fabricated. The developed membranes and modules can be used for industrial gas separations.
- Compared to conventional absorption/desorption technologies, the critical advantage of the HFMC process is the high contact surface area provided by the hollow fibers that enable an increased volumetric mass-transfer rate. In the PEEK HFMC process, the specific surface area has been increased by an order of magnitude over structurally packed or trayed columns, resulting in compact systems with small footprints.
- Energy-efficient, two-stage heated-flash solvent regeneration process was developed and patented. This process can be used in other solvent-based processes.
- The Super-hydrophobic layer of the membrane remained intact. A technique for the infusion of epoxy into fluorinated hollow fibers to secure the fibers into the tubesheet was developed.
- The engineering-scale HFMC system was well designed without major operating issues. The design and operating procedures, representing the largest membrane contactor system for flue gas treating to date, will be helpful for future membrane contactor scaleups.
- Sulfate precipitation in the flue gas has not been reported by other developers at NCCC.
- Membrane contactor CO<sub>2</sub> capture is widely studied by researchers. This project has advanced the HFMC technology to a high TRL and resolved a number of technical issues (e.g. concentration polarization) that other researchers have not dealt with to date. The project results and publications will be a significant contribution to the literature and other technology developers.

## 9. Conclusions and Future Steps

---

- Due to the chemical interaction of CO<sub>2</sub> with the absorption solvent, the permeate side partial pressure of CO<sub>2</sub> can be close to zero. It is, therefore, beneficial to operate the membrane contactor at lower CO<sub>2</sub> partial pressures, conditions that match those of the flue gases.
- The key component of the HFMC process is the super-hydrophobic, porous hollow fiber, which is made from PEEK. The unique characteristics of PEEK allow the HFMC device to be utilized successfully in challenging and aggressive chemical environments which are encountered in the solvent absorption process.
- Compared to conventional absorption/desorption technologies, the critical advantage of the HFMC process is the high contact surface area provided by the hollow fibers that enable an increased volumetric mass-transfer rate.
- The PEEK HFMC has shown high CO<sub>2</sub> capture performance because of the high membrane intrinsic CO<sub>2</sub> permeance as well as the structured PEEK hollow fiber module configuration.
- Solvent selection and HFMC process design are additional parameters that are critical to an energy-efficient CO<sub>2</sub> capture. The PEEK HFMC is compatible with and can operate using commercially available solvents as well as with advanced solvents currently under development.

Future steps would include the following:

- Technical hurdles in materials and manufacturing will need to be resolved in a bench-scale program
- The inner diameter of the hollow fibers should be increased to achieve a low pressure drop (when flue gas flows through the hollow fibers)
- When the technology returns to engineering scale development, approaches to include multiple membrane cartridges in one housing should be considered.

## 10. References

---

1. T. C. Merkel, H. Lin, X. Wei, R. Baker, Power plant post-combustion carbon dioxide capture: An opportunity for membranes, *J. Membr. Sci.* **2010**, 359, 126.
2. S. Khaisri, D. deMontigny, P. Tontiwachwuthikul, R. Jiratananon, Comparing membrane resistance and absorption performance of three different membranes in a gas absorption membrane contactor, *Sep. Purif. Technol.* 65 (2009) 290–297.
3. D. deMontigny, P. Tontiwachwuthikul, A. Chakma, Using polypropylene and polytetrafluoroethylene membranes in a membrane contactor for CO<sub>2</sub> absorption, *J. Membr. Sci.* 277 (2006) 99–107.
4. N. Nishikawa, M. Ishibashi, H. Ohta, N. Akutsu, H. Matsumoto, T. Kamata, H. Kitamura, CO<sub>2</sub> removal by hollow fiber gas-liquid contactor, *Energy Convers. Manage.* 36 (1995) 415–418.
5. D. deMontigny, P. Tontiwachwuthikul, A. Chakma, Comparing the absorption performance of packed columns and membrane contactors, *Ind. Eng. Chem. Res.* 44 (2005) 5726–5732.
6. J.L. Li, B.H. Chen, Review of CO<sub>2</sub> absorption using chemical solvents in hollow fiber membrane contactors, *Sep. Purif. Technol.* 41 (2005) 109–122.
7. J.M.S. Henis, M.K. Tripodi, *Science*, 220 (1983) 11.
8. B. Bikson, Y. Ding, E. G. Krashenninikov, Advances in membrane technology open new options for natural gas treating, 2013 Laurance Reid Gas Conditioning Conference, Norman, Oklahoma, Feb. 24-27, 2013.
9. Y. Yuan, Porous poly (aryl ether ketone) membranes, process for their preparation and use thereof, US Patent 6,887,408, May 5, 2003.
10. Y. Yuan, Y. Ding, Functionalized porous poly(aryl ether ketone) materials and their use, US Patent 7,176,273, Feb 13, 2007

## List of Acronyms

---

aMDEA: Activated Methyldiethanolamine

ALaS: Air Liquide Advanced Separations

DOE: U.S. Department of Energy

FGD: Flue Gas Desulfurization

GC: Gas Chromatograph

GPU: Gas Permeance Units

GTI: Gas Technology Institute or GTI Energy

IPA: Isopropyl alcohol

K-F.: Karl-Fischer Test method

HFMC: Hollow Fiber Membrane Contactor

MDEA: Methyldiethanolamine

MW<sub>e</sub>: Megawatt (electrical)

NCCC: National Carbon Capture Center

NETL: National Energy Technology Laboratory

PC: Pulverized Coal

PEEK: Poly (Ether Ether Ketone)

PEI: Polyether Imide

psig: Pressure in pounds/square inch gauge

QA: Quality Assurance

QC: Quality Control

RCCA: Root Cause and Corrective Action

STP: Standard Temperature and Pressure

TIC: Total Inorganic Carbon

TRL: Technology Readiness Level

wt.%: percentage by weight (generally used for liquid components)

%: percentage by volume (generally used for gaseous components)

**END OF REPORT**